From the:

Comprehensive Pneumology Center (CPC) München
Helmholtz Zentrum Muenchen
and the
Medizinischen Klinik und Poliklinik V
Klinik(um) der Ludwigs-Maximilians-Universität München
Director: Prof. Dr. med. Jürgen Behr

Role of ERBB3 in the interplay between epithelial cells and fibroblasts during late-stage lung development and disease

Thesis for the attainment of the degree of Doctor of Philosophy (Ph.D.)
at the Faculty of Medicine, Ludwig-Maximilians University Munich

Submitted by

Xin Zhang
From Nei Mongol, China

Munich 2022

With the approval of the Faculty of Medicine of the Ludwig-Maximilians University Munich

First evaluator: PD Dr. Anne Hilgendorff

Second evaluator: Dr. Tobias Stöger

Third evaluator: Prof. Dr. Matthias Griese

Fourth evaluator: Prof. Dr. Bianca Schaub

Dean: Prof. Dr. med. Thomas Gudermann

Date of oral defense: 17.11.2022

Table of content

List of tables

Abstract

Background

Lung development is subdivided into 5 stages: embryonic, pseudoglandular, canalicular, saccular, and alveolar stages. The first four stages are completed in the fetal lung through airway branching. About 90% gas exchange area is formed during the last stage of alveolarization by secondary septation, which concludes the coordinated growth of septae from the alveolar walls to subdivide the distal saccules into alveoli, accompanied by microvascular maturation and underlying matrix formation and remodeling. Interplay between the mesenchymal-alveolar epithelial cells is key to understanding the septation process during alveolarization. The epidermal growth factor receptor family (also known as ERBBs) pathways play a crucial role in orchestrating epithelial progenitor cell differentiation and organ maturation. The current study aimed at unraveling the role of ERBB3 in lung development and disease with a specific focus on the epithelial-mesenchymal crosstalk.

Temporal and spatial resolution of ERBB3 signaling

Neonatal Balb/c mice were sacrificed on postnatal day 3, 5, 7, 10, 14, 21, or 60, and their lungs were excised and prepared into formalin fixed paraffin embedded (FFPE) lung slides, and stained for phosphorylated Erbb3 (pErbb3). Data of single-cell RNA-sequencing time-series were obtained from online databases published by collaborating partners and analyzed for gene expression. Phosphorylated Erbb3 receptor level peaked on postnatal day (PND) 5 and remained at a high level until PND14, corresponding to the structural changes of increased alveolar number and enlarged air exchange area featured in postnatal

alveolarization. The Erbb3 is expressed in type 1 alveolar epithelial cells (AEC1) and type 2 alveolar epithelial cells (AEC2) in the lung periphery, co-localized with other crucial components that drive lung scaffold formation, i.e., elastic fiber, and Pdgf-Rα positive fibroblasts at the septal tips in the postnatally developing lung.

Epithelial cells-fibroblasts interaction and underlying pathway crosstalk

An *ex vivo* model of lung organoids was derived from co-culture of primary mouse epithelial cells (PMECs) and murine lung fibroblasts cell line (Mlg) or primary mouse fibroblasts culture) in Matrigel to study the interaction between epithelial cells and fibroblasts. Samples were collected at day-7 or 14 for analysis of morphology and gene expression. Organoids derived from neonatal PMEC + Mlg revealed higher expression of Pdgf-Rα in fibroblasts when compared to the adult organoids, and had increased organoid size. Increased fibroblasts number resulted in organoid segmentation, similar to septation. Supplemental Nrg1 treatment provoked epithelial cell proliferation by Erbb3 activation.

Murine lung epithelial cell line (MLE12) cells were co-cultured with primary fibroblasts in a transwell system for 24h without direct contact. Gene expression was analyzed in both cell types with comparison to monoculture. Cell-cell interaction by soluble molecules resulted in upregulation of neuregulin (*NRG1*) in fibroblasts and *ERBB3* in MLE12 cells, together with upregulation of GATA Binding Protein 6 (*GATA6*), homeodomain-only protein (*HOPX*), Vascular Endothelial Growth Factor A (*VEGFA*), ATP Binding Cassette Subfamily A Member 3 (*ABCA3*), and Collagen Type I Alpha 1 Chain (*COL1A1*). Gene expression in Platelet Derived Growth Factor Subunit A (*PDGF-A*), *NRG1*, and Aquaporin 5 (*AQP5*) remained unchanged.

Impact of moderate hyperoxia exposure on ERBB3 signaling

In vitro monoculture of both MLE12 and primary mouse fibroblasts were exposed to moderate hyperoxia (FiO_2=0.4) for 48h and analyzed for mRNA and protein expression. In a subsequent experiment, supernatant from hyperoxia-exposed fibroblasts was collected to treat MLE12 cells for 12h, and gene analysis was performed in MLE12 cells. Organoids derived from neonatal PMEC and Mlg were cultured under normoxia for 7 days and exposed to hyperoxia for another 7 days, with or without supplemental NRG1 in the medium, and analyzed for morphological changes. Neonatal mice at PND 5-7 were exposed to hyperoxia for 8h and sacrificed for lung protein expression analysis.

After hyperoxia exposure, *ERBB3* was downregulated in MLE12 cells accompanied by decreased proliferation. Likewise, protein level of ERBB3 also decreased in neonatal mouse lungs after hyperoxia exposure. Ligand (NRG1) expression was upregulated in primary wildtype fibroblasts together with PDGF-Rα and COLLAGEN1 expression when co-cultured with MLE12 cells, whereas ACTA2 expression was downregulated. These changes were less prominent in platelet-derived growth factor receptor alpha (PDGF-Rα$^{+/-}$) fibroblasts. Incubation with supernatant derived from hyperoxia-exposed fibroblast cultures did not affect ERBB3 signaling in MLE12 cells. In *ex vivo* organoids, hyperoxia reduced epithelial cell proliferation and organoid expansion, while NRG1 treatment partially counterbalanced the repression effect.

Conclusion

In summary, temporal ERBB3 receptors expression in neonatal mouse lung was most prominent during the postnatal alveolarization period (PND3-14), and

localized at the septal tip in alveolar epithelial cells. Activation of ERBB3 signaling led to epithelial cell proliferation, indicating a crucial role of ERBB signaling in alveolar epithelium elongation during secondary septation. Epithelial cell-fibroblast interaction was essential in activating ERBB3 signaling. Hyperoxia exposure downregulated ERBB3 signaling in epithelial cells and repressed epithelial cell proliferation, and exogenous NRG1 treatment partially counterbalanced the repression.

1. Introduction

1.1 Lung development and growth pathway regulation

1.1.1 Stages of lung development in human and mouse

Based on morphological characteristics, lung development is subdivided into 5 stages: embryonic, pseudoglandular, canalicular, saccular, and alveolar stages (**Fig 1**). The first four stages are completed in the fetal lung through branching of the airway epithelium from lung buds into the surrounding mesenchyme, resulting in the highly ramified tubular networks as well as approximately 10% of gas exchange area in the alveolar ducts and saccules(Metzger et al. 2008; Mund, Stampanoni, and Schittny 2008). The rest 90% gas exchange area is formed during alveolarization stage by secondary septation, which concludes the coordinated growth of septae from the alveolar walls to subdivide the distal saccules into alveoli, accompanied by microvascular maturation and underlying matrix formation of the interstitial scaffold(Schittny 2017; Nikolić, Sun, and Rawlins 2018). In human lung development, the alveolarization stage spans from 36 weeks (gestational age) until young adulthood(Schittny 2017), whereas in mouse this process is considered to begin after birth (postnatal days(PND) 5-30)(Amy et al. 1977). Therefore, lungs from termed neonatal mice serves as an ideal model for late-stage lung development (alveolarization) studies.

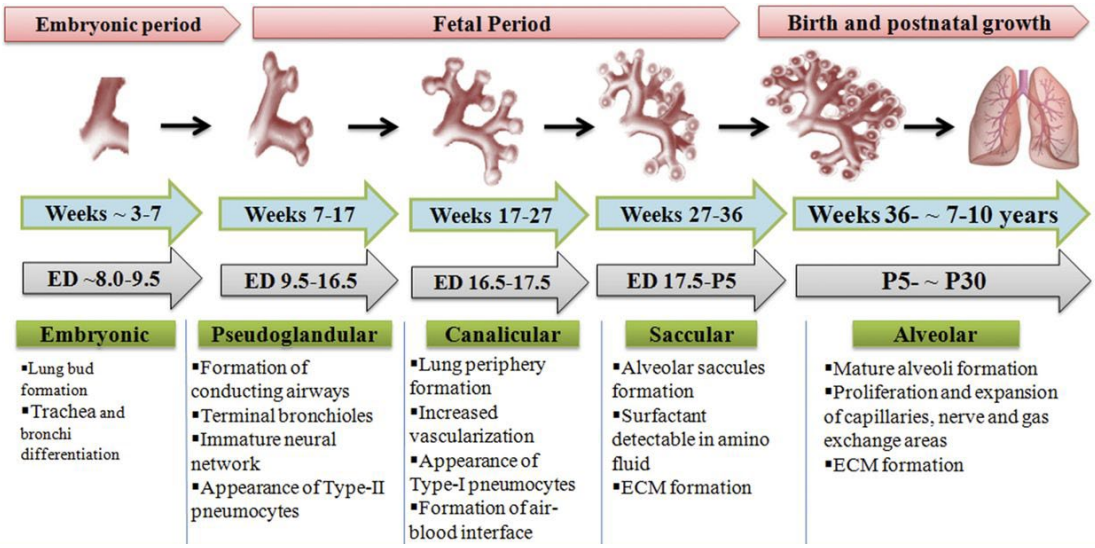

Fig 1. Lung developmental stages and corresponding histological events in humans and mice. adapted from(Hussain et al. 2017).

1.1.2 Secondary septation and underlying growth factor pathway regulation

Secondary septation starts from the uplifting of the saccular wall at locations where elastin is deposited by myofibroblasts. The elastin and collagen fibers stay at the tip of the septa, activate the proliferation of adjacent epithelium and underlying capillaries, and guide the elongation of the secondary septae towards the inner air space(Bonnans, Chou, and Werb 2014; Cybulsky et al. 1999; Lu et al. 2011). The septation is followed by thinning of the septae wall, fusion of double-layered capillaries, as well as extracellular matrix (ECM) remodeling, resulting in an increased number of alveoli and enlarged air space area for air exchange (**Fig 2**).

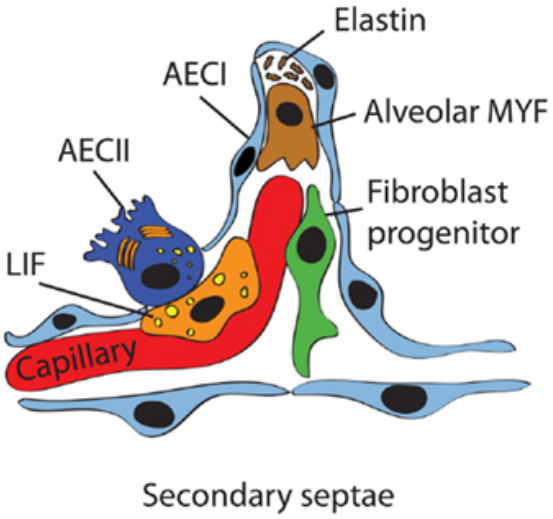

Fig 2. Structure and cell composition of secondary septae during alveolarization, adapted from (Chao et al. 2015)

Three major fibroblast subpopulations have been reported crucial components for the alveolarization process, including myofibroblasts, lipofibroblasts, and matrix fibroblasts. Myofibroblasts are the most studied subtype in the secondary septation, whose differentiation and migration are regulated by platelet-derived growth factor A (PDGF-A) expressed by alveolar epithelial cells(Andrae, Gallini, and Betsholtz 2008; Boström et al. 1996; Yamada et al. 2018). Deficiency in PDGF-A expression leads to reduced myofibroblast population and tropoelastin (precursor of elastin) expression(McGowan et al. 2008; Perl and Gale 2009; Lindahl et al. 1997; Ushakumary, Riccetti, and Perl 2021). Transforming growth factor-β (TGF-β) treatment to the myofibroblasts can activate the transcription of elastin(Kuang et al. 2007). Tenacin and Notch signaling are also involved in the regulation of myofibroblast migration and elastin deposition(Xu et al. 2009; Hussain et al. 2017).

1.1.3 Epithelial cell differentiation during alveolarization

Alveolar epithelial cells, on the other hand, undergo both differentiation and proliferation during septation. Lineage tracing analysis suggests that both alveolar type 1 and type 2 cells (AEC1 and AEC2 cells) arise from the same bipotential progenitor cells located at the bronchoalveolar junction during the saccular stage (**Fig 3**). The bipotential progenitor cells remain the major cell population in air sac epithelium until distinguished by PND4(Desai, Brownfield, and Krasnow 2014; Treutlein et al. 2014). The regulation of airway epithelial cell differentiation and airway branching in fetal lung by fibroblast growth factors (FGF) and Wnt/β-catenin has been extensively studied, whereas the regulation in alveolar epithelial cells is still largely unexplored(Malleske et al. 2018; Volckaert and De Langhe 2015). The FGF10, expressed during E10.5 to E12.5, keeps the undifferentiated status of bronchial epithelial progenitors ($SOX9^+$) by activating β-catenin pathway. The progenitors start to differentiate into bronchial epithelial cells ($SOX2^+$) when FGF10 signaling is decreased in distant airway after branching, and give rise to basal cells, club cells, ciliated cells, as well as neuroendocrine cells(Sivakumar and Frank 2019; Yuan et al. 2018; Ostrin et al. 2018). The Bone Morphogenic Protein 4 (BMP4) expressed at the distal epithelium bud, in association with sonic hedgehog (SHH), antagonizes FGF10 effect in airway branching(Nasri et al. 2021; Weaver, Dunn, and Hogan 2000; Bellusci et al. 1996; Weaver, Batts, and Hogan 2003).

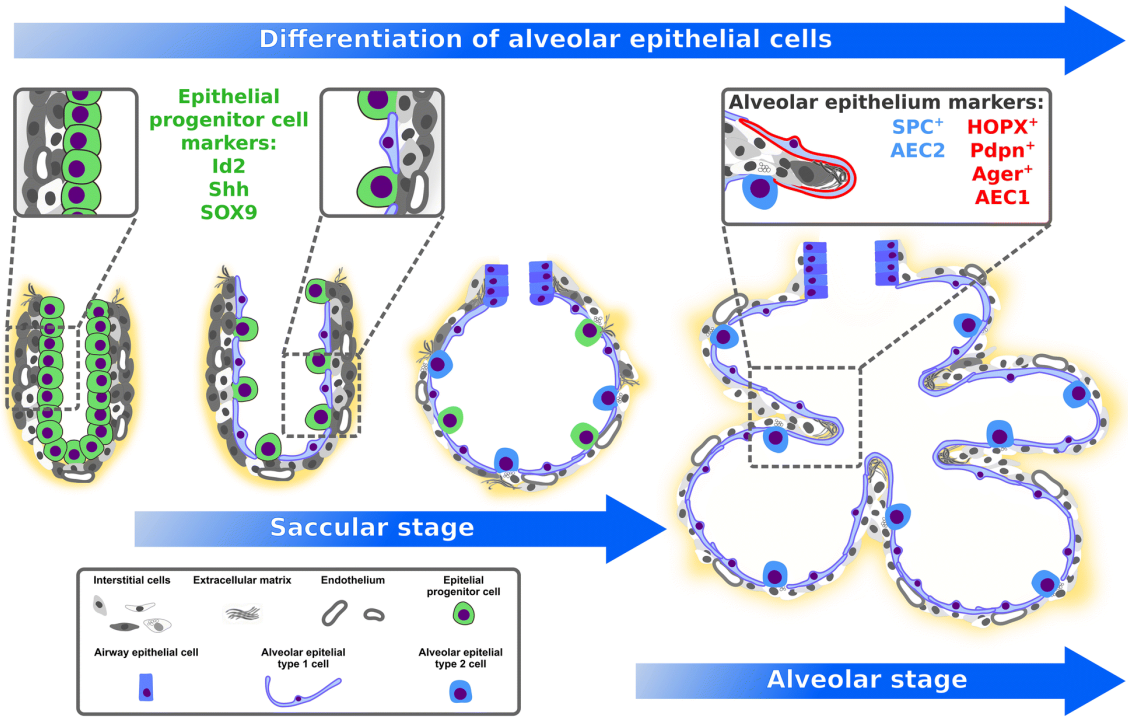

Fig 3. Differentiation of alveolar epithelial cells during saccular and alveolar stages, adapted from (Rodríguez-Castillo et al. 2018).

1.1.4 Bronchopulmonary Dysplasia (BPD) and postnatal hyperoxia injury in preterm infants

Bronchopulmonary dysplasia (BPD) is the most common chronic lung disease in premature infants that results in impaired lung alveolarization and dysregulated vascularization. These babies are born mostly at saccular stage of lung development with immature alveolar structure as well as insufficient surfactant secretion. Various pre- and postnatal factors are known to interfere with the postnatal alveolarization and are intricately interrelated to pathogenesis of BPD, including maternal smoking, chorioamnionitis, genetic susceptibility prenatally, and hyperoxia, mechanical ventilation, infection postnatally(Kalikkot Thekkeveedu, Guaman, and Shivanna 2017; Morrow et al. 2017). In this study, we laid particular focus on the molecular mechanism of hyperoxia injury induced pathway dysregulation.

1.2 Models for cell-cell interaction study

1.2.1 *In vitro* co-culture system

Interplay between the mesenchymal-alveolar epithelial cells is the key in understanding the septation process during alveolarization. There have been several types of co-culture models set up to study cell-cell interaction. In co-culture models that allow for cell-cell contact, fetal mouse lung mesenchyme with A549 epithelial cells produced protrusion of mesenchymal cells covered by epithelial cells resembling the secondary septae, but not with adult mesenchymal cells(Greer et al. 2014). Non-contacting co-culture of the human mesenchymal stem cells (MSCs) with small airway epithelial cells (AE) increased the viability of the AE, as well as gene expression of intercellular adhesion molecule 1 (*ICAM1*) and mucin (*MUC1*)(Schmelzer et al. 2020). In the current study, we employed a non-contacting transwell system, which allows bidirectional diffusion of soluble signaling molecules in between, to elucidate the pathway crosstalk between the mesenchymal-alveolar epithelial cells during lung development.

1.2.2 *Ex vivo* organoids

The ECM not only provides scaffold support for the growth and migration of mesenchymal and epithelial cells, but also modulates the differentiation of progenitor epithelial cells and cell-cell interaction. Supplemental collagen and laminin-5 (LN5) help preserve the AEC2 phenotype in isolated primary AEC2 cells(Olsen et al. 2005; Daley and Yamada 2013; Lwebuga-Mukasa 1991). Built on knowledge from the *in vitro* co-culture assay, we then established a 3D culturing model of primary epithelial cells and fibroblasts embedded in matrigel, mirroring the geometrical and biological context in the developing lung periphery. The matrigel is a solubilized basement membrane matrix secreted by Engelbreth-Holm-

Swarm (EHS) mouse sarcoma cells, and contains Laminin (major component), Collagen IV, heparan sulfate proteoglycans, and entactin/nidogen. Cellular and molecular behavior study in this model can provide information on cell type specific crosstalk among fibroblasts and epithelial progenitors-derived cells. The *ex vivo* model is amendable to specific pathways modulation and therefore can provide insight into the pathway interaction in the interplay between mesenchymal-epithelial cells.

1.3 ERBB3 pathway signaling

1.3.1 The epidermal growth factor family

The epidermal growth factor receptor (EGFR) family consists of four transmembrane receptors: EGFR (also known as ERBB1 or HER1), ERBB2 (HER2), ERBB3 (HER3) and ERBB4 (HER4). Similar to other receptor tyrosine kinase (RTK) proteins, the ERBB receptors are also comprised of a ligand-binding extracellular domain, an α-helix transmembrane segment, an intracellular domain consisting juxtamembrane domain, a typical tyrosine protein kinase segment, and a tyrosine-rich carboxyterminal tail(Appert-Collin et al. 2015).

In the absence of a ligand, the receptor exists on the plasma membrane as a monomeric transmembrane protein with its extracellular part tethered by domain II and IV. Ligand binding to the extracellular domain changes the receptor into activated conformation and triggers the dimerization of ERBB receptors to form homo or heterodimers with another ERBB receptor. Dimerization consequently activates the intrinsic tyrosine kinase activity and triggers autophosphorylation of specific tyrosine residues on the carboxyterminal tail of the receptor. The phosphorylated residues provide docking sites for downstream proteins and a

signaling cascade is initiated (**Fig 4**)(Olayioye et al. 2000; Schulze, Deng, and Mann 2005; Tao and Maruyama 2008). Although all the four ERBB members share similar patterns of structural and conformational characteristics, there are some substantial differences among them. While EGFR and ERBB4 are fully functional, ERBB2 has no ligand binding ability and ErbB3 lacks intrinsic functional kinase domain, which contributes to the fact that homo and heterodimers of different combination retain varied affinity to the epidermal growth factors (EGF) family of ligands. Consequently, both ERBB2 and ERBB3 are only active in the heterodimer context(Citri, Skaria, and Yarden 2003; Sliwkowski et al. 1994; Váradi et al. 2019; Lemmon 2009) (**Fig 5**). Despite the extensive studies done with EGFR members in oncology, both the molecular mechanism of ERBB3 activation and its physiological consequence remained poorly understood. The current study aimed at unraveling the role of ERBB3 in lung development and disease.

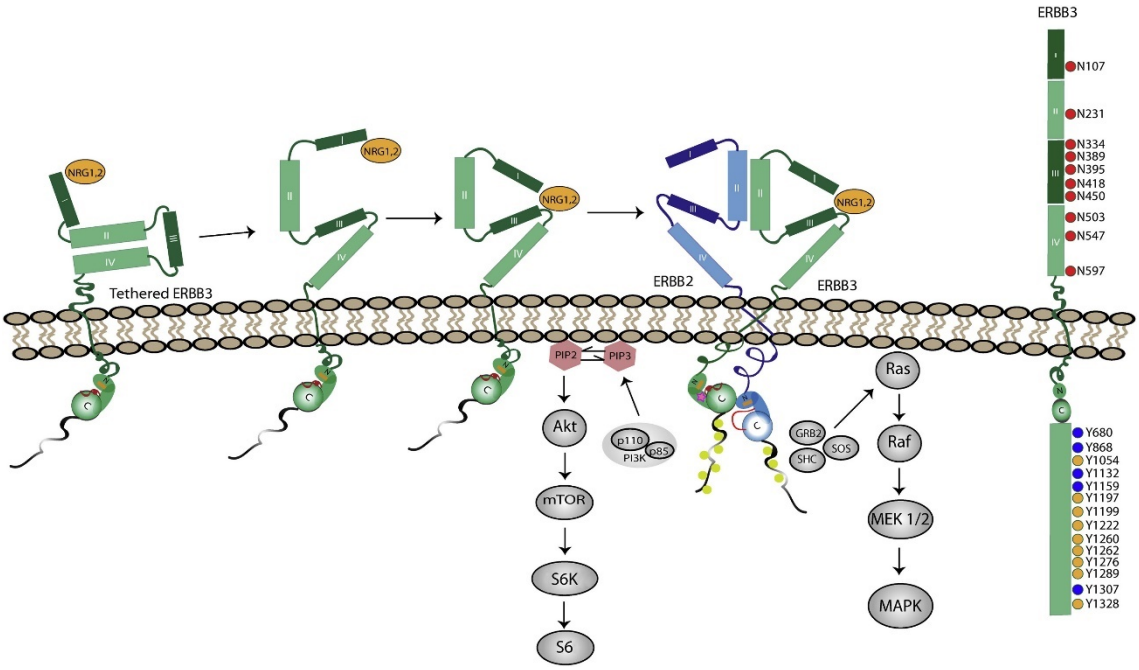

Fig 4. Schematic of ERBB3 conformational change upon ligand activation, adapted from (Black, Longo, and Carroll 2019)

1.3.2 Ligands for ERBB receptors

The ERBB receptors are activated by a family of at least 11 ligands that share the same EGF like domain. These ligands have varied affinity to the ERBB family members (except for ERBB2) (**Fig 5**) as well as divert signaling outcomes. The neuregulins (NRG) proteins are synthesized and released by proteolysis as transmembrane proteins that are comprised of EGF-like domain, transmembrane domain and intracellular domain. The NRG1 proteins are divided into 6 isomers by different slicing, and only NRG1 and NRG2 can activate ERBB3. We chose NRG1 in the current study based on its abundant tissue distribution in lungs comparing to NRG2(Nagasaka and Ou 2022).

The extracellular EGF-like domain of NRG1 is shedded into extracellular environment and acts on ERBB receptors via autocrine or paracrine. Tissue distribution and shedding of the ligands is therefore crucial for the pathway modulation. Studies have shown that Metalloprotease ADAM17/TACE and ADAM19/meltrin-β are responsible for shedding of the NRG1 ectodomain(Spanò and Scilabra 2022; Herrlich et al. 2008; Higashiyama et al. 2011; Iwakura et al. 2017). Stimulus such as extracellular Ca^{2+} influx, Interleukin 6, inflammation is correlated with the NRG1 shedding and ERBB pathway activation(Mishra et al. 2019; Finigan et al. 2013).

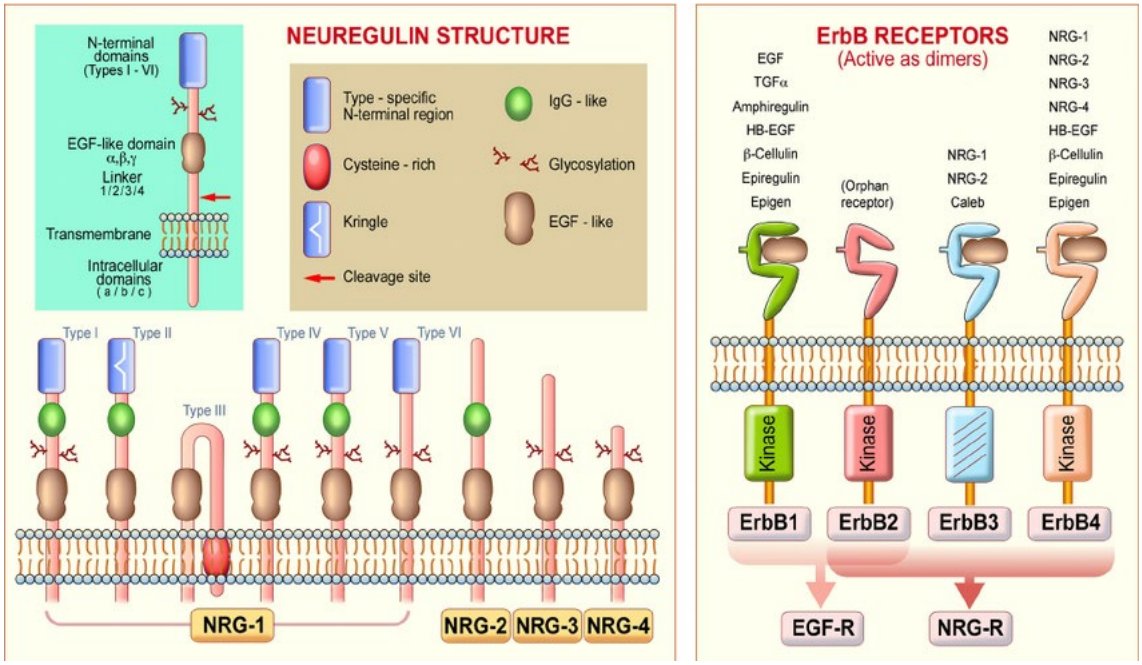

Fig 5. Structures of Neuregulin subtypes and binding to ERBB receptors, adapted from (Gumà et al. 2010).

1.3.3 ERBB signaling in development

ERBB receptors signal through the mitogen-activated protein kinase (MAPK)/ extracellular signal-regulated kinases (ERK) and the phosphatidylinositol 3-kinase (PI3K)-AKT pathways to regulate cell proliferation, migration, differentiation, apoptosis, and cell motility. Studies in neonatal lung revealed that ERBB4 is essential for surfactant synthesis in AEC2 cells(Fiaturi, Castellot, and Nielsen 2014), and regulates stretch-induced type II cell differentiation via ERK pathway together with EGFR(Huang et al. 2012). Knockout of either *ERBB2* or *ERBB3* lead to lethality at embryonic stage (E10.5 for *ERBB2*, E13.5 for *ERBB3*)(Lee et al. 1995; Riethmacher et al. 1997) with deficiencies in cardiac valve and neural crest formation and lack of Schwann cell precursors. These results suggest that ERBB pathways play a crucial role in the process of progenitor cell differentiation and organ maturation.

2. Hypothesis and aims

In the process of alveolarization, the complex interplay between different cell types and their characteristic signaling pathways drive septation, functional alveolar maturation and formation of the vascular bed. The pathway crosstalk between fibroblasts and alveolar epithelial cells mediates the proliferation and differentiation process. The ERBB pathways play a crucial role in the process of epithelial progenitor cell differentiation and organ maturation. Despite the extensive studies done with EGFR members in oncology, both the molecular mechanism of ERBB3 activation and its physiological consequence remained poorly understood. The current study aimed at unraveling the role of ERBB3 in lung development and disease.

The hypothesis of this study is that ERBB3 regulates the proliferation and differentiation of alveolar epithelial cells during late-stage lung development and directs the secondary septation through ERBB3-PDGF crosstalk with peripheral parenchymal cells. Postnatal lung injury by hyperoxia exposure dysregulates ERBB3 signaling, resulting in impaired alveolarization.

We defined the following sub steps:

1) Define the temporal, spatial, and cell specific resolution of ERBB3 expression in neonatal lung.
2) Elucidate ERBB3 regulation and crosstalk with PDGF in models of epithelial-mesenchymal cell co-culture.
3) Investigate impact of hyperoxia exposure on ERBB3 signaling

3. Material and Methods

3.1 Reagents and antibodies

Recombinant Human NRG1-beta 1/HRG1-beta 1 EGF Domain Protein was re-constituted at 100 µg/mL in sterile PBS containing 0.1% bovine serum albumin (PAN-Biotech, P40-1302) as stock solution and further diluted with cell culture medium to target concentration.

Table 1 Chemicals used for staining and cell culture

Product	**Ref No.**	**Manufacturer**
Saponin	A18820.14	VWR International
Gelatin powder	24350.262	VWR International
THIMEROSAL	PHR1587-1G	Sigma-Aldrich
Dispase	354235	BD biosciences
Mitomycin C	M4287	Sigma-Aldrich

Table 2 Primers used in qPCR:

Gene	**Species**	**Primer Sequence (5' to 3')**	
Erbb3	mouse	Forward	GGGCTTCTCCTTGTT
		Reverse	CGCAGAAGTCTGGTC
Nrg1	mouse	Forward	ATCGCCCTGTTGGTGGTCGG
		Reverse	AGCTTCTGCCGCTGTTTCTTGGT
Abca3	mouse	Forward	CAGCTCACCCTCCTACTCTG
		Reverse	ACTGGATCTTCAAGCGAAGCC
Col1a1	mouse	Forward	CCAAGAAGACATCCCTGAAGTCA
		Reverse	TGCACGTCATCGCACACA

Gene	Species	Primer Sequence (5' to 3')	
Acta2	mouse	Forward	CGAAACCACCTATAACAGCATCA
		Reverse	GCGTTCTGGAGGGGCAAT
Vegfa	mouse	Forward	GCAGATGTGAATGCAGACCAAA
		Reverse	GGTTAATCGGTCTTTCCGGTG
Pcna	mouse	Forward	ACCTGCAGAGCATGGACTCGT
		Reverse	TTGGACATGCTGGTGAGGTTCAC
Gata6	mouse	Forward	ACGCCTCTGCACGCTTTCCC
		Reverse	GCCGCCACCTCCACTCACAC
Pdgfra	mouse	Forward	AGGTATGTATCCACACA TGCGT
		Reverse	AGTTCCTGTTGGTTTCA TCTCG
Pdgfa	mouse	Forward	TGTGCCCATTCGGAGGAA
		Reverse	GAGGTATCTCGTAAATGACCGTC
Hprt	mouse	Forward	CCTAAGATGAGCGCAAGTTGAA
		Reverse	CCACAGGACTAGAACACCTGCTA
Hopx	mouse	Forward	TCTCCATCCTTAGTCAGACGC
		Reverse	GGGTGCTTGTTGACCTTGTT

Table 3 Primary antibodies used in immunohistochemistry, immunofluorescence, and immunoblot

Antibody against	Host Species	Dilution	Manufacturer	Ref No.	Application
ERBB3	Rabbit	1:1000	Mybiosource	MBS8305698	WB
NRG1	Mouse	1:50	Santa Cruz	sc393006	WB
COLLA-GEN1	Rabbit	1:1000	Abcam	Ab34710	WB
PERBB3 (Y1222)	Rabbit	1:100 1:1000	Mybiosource	MBS9610623	IHC WB
KI67	Rabbit	1:200	Abcam	ab16667	IHC

Antibody against	Host Species	Dilution	Manufacturer	Ref No.	Application
HOPX	Rabbit	1:50	Santa Cruz	sc30216	IF
PDGFRA	Rabbit	1:100	Cell signaling	3174	IF
SP-C	Rabbit	1:100	Merck Millipore	AB3786	IF
PDPN	Hamster	1:200	Abcam	Ab11936	IF
A-TUBULIN	Rabbit	1:100	Abcam	Ab179484	IF
A-SMA	Goat	1:100	Abcam	Ab21027	IF

Table 4 Secondary antibodies used in immunohistochemistry, immunofluorescence, and immunoblot

Antibody against	Dilution	Manufacturer	Ref No.	Application
Goat anti-Rabbit IgG (H+L) Alexa Fluor 488	1:800	Thermo	A-11034	IF
Goat anti-Hamster IgG (H L) Cross-Adsorbed Secondary Antibody, Alexa Fluor 647	1:800	Thermo	A-21451	IF
Goat anti-Mouse IgG (H+L) Highly Cross-Adsorbed Secondary Antibody, Alexa Fluor Plus 555	1:800	Thermo	A-32727	IF
Mouse anti-rabbit IgG-HRP	1:1000	Santa Cruz	sc-2357	WB
Goat anti-mouse IgG HRP	1:1000	Santa Cruz	Sc-2005	WB
Goat anti-Rabbit SignalStain® Boost Detection Reagent	/	Cell signaling	8114	IHC

3.2 Cell lines and culture techniques

3.2.1 Cell lines

Murine lung epithelial cell line (MLE 12, ATCC CRL-2110) and murine lung fibroblasts cell line (MLg, ATCC, CCL-206) cells were cultured with Dulbecco's Modified Eagle Medium/Nutrient Mixture F-12 (DMEM/F-12, Gibco), supplemented

with 10% (v/v) fetal bovine serum, FBS (PAN-Biotech), 0.5 mg/mL Gentamicin, 50 µg/mL penicillin, and 50 U/mL streptomycin (Gibco). Each cell line was expanded in polystyrene (PS) T-75 cm^2 flasks (Thermo Fisher Scientific) and grown in a CO_2 cell Incubator BBD6620 (Thermo Fisher Scientific) with humidified conditions at 37°C and 5% CO_2. Culturing medium was renewed every two days. For subculturing, cells were rinsed with 1x PBS and incubated with 4 mL of 0.25 % Trypsin-EDTA for 2 min at 37°C and observed under microscope until cell layer was dispersed. Trypsin activity was neutralized with 10 mL of complete DF12 growth medium. Cells were suspended by gentle pipetting. The cell suspension was then aliquoted to new flasks at a ratio of 1:5. For cryopreservation, cell suspension containing approximately 1×10^7 cells were centrifuged and resuspended in freezing medium containing 5% (v/v) dimethyl sulfoxide, DMSO (Carl Roth) in complete growth medium, and kept in a Liquid nitrogen cell tank BioSafe 420SC (Cryotherm). Cell numbers were calculated using a Neubauer chamber, trypan blue 0.4% solution (Sigma-Aldrich) at a 1:10 dilution and the following formula: cell concentration (number of cells/mL of cell suspension) = (number of cells counted × 10,000) /number of squares counted. For all liquid pipetting volumes, either sterile measuring pipettes (Greiner bio-one) of single use (5 mL, 10 mL, 25 mL, 50 mL) were used with the help of PIPETGIRL (Integra), or filter tips (Biozym Scientific) were used (10 µL, 100 µL, 200 µL and 1000 µL) with fixed volume, single channel Research Plus pipettors (Eppendorf). To achieve sterile conditions, tissue culture was performed under a laminar flow hood Herasafe KS (Thermo Fisher Scientific).

3.2.2 Mouse primary pulmonary fibroblasts

Neonatal C57BL/6J mice (Jax #000664) and PDGF-Rα$^{+/-}$ mice (B6.129S4-Pdgfra$^{tm11(EGFP)Sor}$/J) at postnatal age of 5-7(PND 5-7) days were sacrificed by intraperitoneal injection of pentobarbital (150 µg/g bw). The lungs were excised and minced into ~1mm^3 pieces, transferred to TC-treated culture dishes (Corning, 430167) and incubated for 5-10min at 37°C for attachment, and then cultured in complete growth media (high glucose Dulbecco's Modified Eagle Medium, DMEM, supplemented with 10% (v/v) fetal bovine serum, FBS (PAN-Biotech), GlutaMAX (Gibco), 0.5 mg/mL Gentamicin, 50 µg/mL penicillin, and 50 U/mL and streptomycin (Gibco)) at 37°C. The media was changed every 2-3 days. Minced tissue was removed after 7-day of culture. The cultured cells were used for further assays when they reach 80-85% of confluence. Cell composition of the fibroblasts culture was characterized by fluorescence-activated cell sorting (FACS LSRII) as reported previously. The fibroblast culture constituted myofibroblasts (77.2 ± 14% PDGF-Rα$^+$/VIMENTIN$^+$, 16.7 ± 12% VIMENTIN$^+$, and 77.6 ± 27% αSMA$^+$), mesenchymal-like cells (8.5 ± 4.5% CD105$^+$, 32 ± 8.6% CD90$^+$), and leukocytes (0.6 ± 0.5% CD45$^+$)(Oak et al. 2017).

3.2.3 Hyperoxia treatment assay

The MLE12 cells were seeded in 6-well plates and cultured until 80%-90% confluency, and then transferred to an incubator with oxygen concentration maintained at 40% for 24h and the rest conditions remain the same (37°C, 5% CO_2, humidified). The cell samples were collected at the end of hyperoxia exposure for RNA extraction.

3.2.4 Epithelial cell-myofibroblasts Co-culture assay

The MLE12 and primary fibroblasts were co-cultured using the Corning polycarbonate membrane transwell (Corning, CLS3396) system. The MLE12 cells were seeded on the bottom of 6-well plate and primary fibroblasts on the transwell membrane and cultured separately until the cells reach 80%-90% confluency. Culturing conditions as described in 2.2.1. The two cell populations were then cultured together for 24h until sample collection.

3.2.5 Supernatant treatment assay

Mouse primary fibroblasts were exposed to 21% or 40% O_2 for 48h, and supernatant were collected from the culture at the end of the exposure and transferred to MLE12 cell cultures. The MLE12 cells were treated for another 24h before sample collection and qPCR analysis.

3.3 Mouse lung organoids culture and readout assays

3.3.1 Primary epithelial cell isolation

Neonatal C57BL/6J mice (Jax #000664) at PND5-7 were sacrificed by intraperitoneal injection of pentobarbital (150 µg/g bw). The entire lungs were excised and flushed with phosphate-buffered saline (PBS) to remove blood residue, and then minced with scalpel and digested with Dispase (BD Bioscience) for 45min at 37°C. The digested lung mixture of 3-4 animals were pooled together and filtered through 100 µm and 40 µm cell strainers (Corning, FALC352360 and FALC352340) successively with the help of syringe pastel. Cell suspension was centrifuged for 10min, 200 RCF, at 15°C between each filtration and resuspended with DMEM medium. Red blood cells were removed by RBC lysis solution (130-094-183). Lung epithelial cells were then isolated by removing white blood cells

and endothelial cells with CD45 and CD31 magnetic beads respectively (Miltenyi Biotec, 130–052-301, 130–097-418) according to manufacturer's instructions.

3.3.2 Organoid culture

Mlg cells were cultured as described in 2.2.1. Before organoids seeding, the Mlg cells were treated with 10µg/mL mitomycin C (Merck) at 37°C for 2h, washed 3 times in warm PBS and let to recover in growth medium for 1h, in order to inhibit the cell proliferation of fibroblasts in the co-culture system. Primary epithelial cells and Mlg cells were suspended in 50% growth factor-reduced Matrigel (Corning, FALC354230), and seeded into 24-well plate tissue culture treated transwell inserts (Corning) with 0.4 µm pore size, made from polyester (PET) membrane, growth area 0.3 cm² and 6.4 mm diameter. The organoid cultures were maintained in DMEM/F12 supplemented with l penicillin (50 µg/mL) and streptomycin (50 U/mL), 1 x GlutaMAX (Gibco), 2.5 µg/mL amphotericin B (Gibco), 1x insulin-transferrin-selenium (Gibco), 0.025 µg/mL recombinant human epidermal growth factor, EGF (Sigma), 0.1 µg/mL cholera toxin (Sigma-Aldrich), 30 µg/mL bovine pituitary extract (Sigma-Aldrich) and 0.01 µM of freshly added retinoic acid (Sigma-Aldrich). Culturing medium was added directly to the bottom of each well beneath the inserts. For the first 48h of culture, 10 µM ROCK inhibitor (Sigma, Y-27632) was added to the medium. Media was refreshed every 2-3 days.

3.3.3 Organoid treatment assay

Organoids were either exposed to hyperoxia (FiO_2=0.4) or treated with NRG1 (80 ng/mL) added to the organoid media since day 8 of culture and refreshed every 2-3 days together with the medium change.

3.3.4 Organoid morphology quantification

Live organoids cultured in the transwell inserts after 7 and 14 days were placed under a Zeiss AxioObserver Z1 microscope equipped with an incubating chamber set at 37°C, 5% CO_2, humidified. Brightfield images from multi-layer Z-stacks were taken covering the thickness of the Matrigel and processed by ImageJ. Each organoid with a minimum diameter of 50 µm was manually circled and calculated for the Ferret diameter and area. The colony forming efficiency (CFE) was calculated by numbers of spheres/numbers of progenitor cells × 100%.

3.3.5 Cellular composition analysis with immunofluorescent staining

3.3.5.1 Sample processing

Organoids cultured in transwell inserts were collected on Day 14, washed twice with PBS and fixed with 2% paraformaldehyde + 0.1% glutaraldehyde in PBS for 15min at 4°C, washed again with PBS, and stored at 4°C for further staining steps.

3.3.5.2 3D staining of organoids

Fixed organoids were permeabilized with 0.5% Triton in PBS for 15min, washed 3×10min, and blocked with goat serum diluted at 1:20 with 0.1% Triton in PBS at 4°C overnight. After blocking, organoids were incubated with primary antibody diluted in 5% serum solution at 4°C overnight, washed 3×10min, and incubated with corresponding secondary antibody and DAPI at 4°C overnight. The stained transwell membranes were washed 3×10min, removed from the transwell and mounted on glass slides with mounting medium (CS703, Dako) for imaging. Immunofluorescence was visualized using either an inverted Zeiss LSM 710 confocal microscope or a Leica SP8 multi-photon microscope. The Z-stacked images were processed with Imaris 9.3.1.

3.3.6 Gene expression analysis

Organoids cultured in transwell inserts were collected at schedule time points (day 7 or 14 of culture), washed twice with PBS, and lysed with RNA lysis buffer from RNeasy Plus Kits (Qiagen) for 5min at 4°C, and proceeded to the following steps described in 2.5.1. Gene expression level was examined by qPCR as described in 2.5.2.

3.4 Animal experiments

3.4.1 Approval of animal experiments

All animal experiments were conducted under strict governmental and international guidelines under protocol ROB-55.2-2532.Vet_02-18-35 and were approved by the local government for the administrative region of Upper Bavaria.

3.4.2 Animal strains, breeding, and maintenance

For breeding, specific pathogen-free (SPF) male and female Balb/c, C57BL/6, and transgenic mice were purchased from Charles River (Sulzfeld, Germany) and Jackson Laboratory (Bar Harbor, Maine, USA), and placed in rooms with constant temperature and humidity at a 12h light cycle for 7 days before mating. Food and water were provided ad libitum for mice.

3.4.3 Gene-targeted PDGF-Rα haploinsufficient (PDGF-Rα$^{+/-}$) mice

Gene-targeted heterozygous mice (B6.129S4-Pdgfra$^{tm11(EGFP)Sor}$/J) were obtained from Jackson laboratories (#007669, Bar Harbor, Maine, USA). Heterozygous mice were healthy and reported with no abnormal pulmonary phenotype(Hamilton et al. 2003). For breeding, heterozygous male mice were mated with wild type (WT) female mice in order to avoid any effect of PDGF-Rα$^{+/-}$ i.e.,

perinatal lethality due to skeletal and pulmonary problems, on the course of the pregnancy(Betsholtz 1995). Pre and postnatally, PDGF-Rα$^{+/-}$ and WT neonatal mice were subjected to identical conditions.

3.4.4 Postnatal lung development analysis in termed Balb/c mice

Neonatal Balb/c mice were randomly selected from multiple litters and assigned to each group. Selected mice were then euthanized with pentobarbital (150 µg/g body weight) at one of the following time point: postnatal day 3, 5, 7, 10, 14, 21, or 60 and sacrificed for sample collection. The lungs were excised, flushed with PBS, and fixed with 4% paraformaldehyde (PFA) diluted with PBS overnight at 4°C. The fixed lungs were then transferred into PBS solution before further processing into formalin fixed paraffin embedded (FFPE) lung slides.

3.4.5 Postnatal mechanical ventilation and hyperoxia exposure in WT and PDGF-Rα$^{+/-}$ heterozygous mice

Neonatal mice at PND 5-7 were randomly assigned to room air or hyperoxia exposure group (6/ group), and exposed to 21% or 40% O_2 for 8 h. A warm and humidified environment was provided for the neonatal mice during the exposure. At the end of exposure, pups were euthanized with an intraperitoneal overdose of sodium pentobarbital, ~150 µg/g bw, and lungs were excised for various studies as described above. All animals were viable with response to tactile stimulation at the end of each experiment.

3.4.6 Animal lung sample collection and processing

Lungs from animals exposed to 8h treatments (Hyperoxia and/or Mechanical ventilation) were either snap frozen in liquid nitrogen and stored at -80°C for further protein and RNA extraction, or fixed with 4% paraformaldehyde (PFA) and

employed for immunohistochemistry and immunofluorescence analysis. Tracheotomy was performed on sedated mice at the end of the 8h-treatment, via insertion of a plastic catheter in trachea to slowly inject 150 µL of 4% PFA to the lungs and kept PFA infusion pressure at 20 cm H_2O pressure overnight at 4°C(Bland et al. 2008). The lungs were removed by an excision in the thorax. The lungs were immersed in 4% PFA for another 24h at 4°C, and dehydrated by tissue processor machine (MICROM STP 42OD, Thermo Scientific) overnight where the lungs were incubated for, 1h 70% ethanol, 1h 80% ethanol, 1h 96% ethanol, 2× 2h 96% ethanol, 1h 100% ethanol, 2×2h 100% ethanol, 1h xylene (Applichem Panreac, 131769.1612), continued with 3h of incubation in paraffin. After dehydration the lungs were embedded in paraffin. Sectioning was accomplished by using a cutting apparatus called microtome (HYRAX M55, ZEISS) with reported IUR randomization method to avoid stereological bias (Mattfeldt, Möbius, and Mall 1985). The thickness of the sections was adjusted to 4 µm for viewing with a light microscope.

3.5 RNA analysis

3.5.1 RNA extraction and cDNA synthesis

Fresh lung tissue was snap frozen in liquid nitrogen and stored at −80°C until further processing. Fresh cells were washed with PBS twice before frozen at −80°C. Total RNA from cells was isolated using the RNeasy Plus Kits (Qiagen), according to the manufacturer's instructions. The RNA concentration was quantified using a NanoDrop 1000 (PeqLab). The RNA samples were diluted to 50 µg/µL with RNase/DNase free water (Gibco) and denatured at 72°C for 10min in a Mastercycler nexus (Eppendorf). The cDNA was synthesized by reverse transcription, using 2.5 U/µL M-MLV Reverse Transcriptase (Invitrogen), 1× First

Strand Buffer (Invitrogen), 10 mM DTT (Invitrogen), 2.5 µM random hexamers (Invitrogen), 0.5 mM of nucleotide (dNTP) mix (Thermo Scientific), and 1 Unit/µL RNase inhibitor (Thermo Scientifics). Incubation at 20°C for 10min was followed by an annealing cycle at 43°C for 75min and an extension at 99°C for 5min and left at 4°C for cooling down in a PCR reaction. The cDNA was diluted 1:5 with RNase/DNase free water and stored at -20°C.

3.5.2 quantitative real-time PCR

The mRNA expression of target genes was analyzed using SYBR Green (Roche) and a LC480 Light Cycler (Roche) and normalized by reference gene hypoxanthine-guanine phosphoribosyl transferase (Hprt)-1. Primers were diluted with RNase/DNase free water to a final concentration of 500 nM. The qPCR reactions were conducted as follow: initial denaturation at 95°C for 5min, followed by 45 cycles of denaturation at 95°C for 5s, annealing at 59°C for 5s and elongation at 72°C for 10s, followed by a cycle of melting curve analysis to acquire the dissociation characteristics of double-stranded DNA at 95 °C for 5s, 1min at 60°C and a continuous acquisition from 60°C to 95°C, ending and a final cooling step at 4°C. Relative transcript expression of a gene was calculated as difference between cycle threshold, ct (ΔCt = Ct reference gene – Ct target gene).

3.6 Protein analysis

3.6.1 Immunohistochemistry

3.6.1.1 Staining of lung tissue slides

The formalin fixed paraffin embedded (FFPE) lung slides from animal *in vivo* studies were deparaffinized by the following steps: 2×5min xylene (Applichem Panreac, 131769.1612), 2×2min 100% ethanol, 1min 90% ethanol, 1min 80%

ethanol, 1min 70% ethanol, 30s dH2O. Slides were then submerged in EDTA unmasking solution(#14747, SignalStain®) for antigen retrieval with at a sub-boiling temperature (95-98°C) for 10min, incubated with 0.5% Tween 20 in PBS for 10min room temperature (RT) to increase membrane permeability, and 3% hydrogen peroxide in PBS for 15min RT to block endogenous peroxidase activity, and washed between each steps with 0.1% Tween 20 in PBS (PBST wash buffer), 3×5min, followed by blocking with goat serum diluted in PBST (1:20 v/v) for 1h, RT. After removing the blocking serum, slides were incubated with primary antibody diluted in antibody diluent (# 8112, SignalStain®) overnight at 4°C, and then with HRP conjugated boost IHC detection reagent (#8114, #8125, SignalStain®) for 30min RT, washed between each step with PBST, 3×5min. The DAB Chromogen (#8059, SignalStain®) was added on the slides and incubate for 2-5min until chromogenic reaction was visible. Slides were counterstained with hematoxylin (#14166, Cell Signaling), dehydrated in the reversed order of dehydration described above, and mounted with mounting medium (S3023, Dako).

3.6.1.2 Quantification

Stained slides were imaged with a brightfield microscope Axio Imager M2 (Zeiss) at 200× magnification. Areas of alveolar and terminal bronchial were selected manually in each picture with ImageJ, and quantification was performed on 3 pictures (sized 447.63×335.40 μm^2) taken from each tissue sections per animal, 3 animals per group with the IHC toolbox in ImageJ.

3.6.2 Immunofluorescence

3.6.2.1 IF stain in 2D slides of cells/lung tissue section

The formalin fixed paraffin embedded (FFPE) lung slides were deparaffinized and incubated for antigen retrieval as described in 2.6.1. Slides with fixed cells start

directly from the permeabilization step: Slides were incubated with 0.5% Tween 20 in PBS for 10min RT, washed with PBST wash buffer, 3×5min, followed by blocking with goat serum diluted in PBST (1:20 v/v) for 1h, RT. After removing the blocking serum, slides were incubated with primary antibody diluted with 5% goat serum in PBST overnight at 4°C, followed by 1h incubation with corresponding secondary antibody and DAPI diluted in 5% serum at RT, and washed 3 times between each step. Slides were mounted with mounting medium (CS703, Dako) in the last step.

3.6.2.2 Tissue clearing and 3D light sheet fluorescent microscopy

The lung tissue samples were fixed in 4% paraformaldehyde at 4 °C overnight and then incubated in PBSG-T (0.2% gelatin, 0.01% thimerosal and 0.5% TritonX100 in PBS) for 3 days with rotation (70 rpm) at RT to block nonspecific antibody binding. Lung samples were incubated with primary antibody diluted in 0.1% Saponin in PBSG-T for 7 days with rotation (70 rpm) at RT. Afterwards, lung samples were rinsed 6 times with PBST (0.5% Triton in PBS) for 1 hour each and incubated with the secondary antibody / 4,6-diamidino-2-phenylindole (DAPI) diluted in 0.1% Saponin in PBSG-T for 3 days with rotation (70 rpm) at RT. Samples were washed 6 times in PBST for 1 hour each with rotation at RT. Tissue clearing was performed after dehydration in an ascending tetrahydrofuran (THF, Sigma, Burlington, MA, United States) series (50% v/v THF/H_2O overnight, 50% THF/H_2O 1h, 80% THF/H_2O 1h, 100% THF 1h, 100% THF overnight, and 100% THF 1h) with mild shaking. Samples were gently dried on tissue paper and then incubated in dichloromethane (DCM, Sigma, Burlington, MA, United States) for 30min and eventually immersed in dibenzyl ether (DBE, Sigma, Burlington, MA, United States) for at least 2h prior to imaging. Imaging was performed in DBE

with an LSFM (Ultramicroscope II, LaVision Biotec) equipped with a sCMOS camera (Andor Neo, Abingdon, United Kingdom) and a 2× objective lens (Olympus MVPLAPO 2×/0.5 NA) equipped with an Olympus MVX-10 zoom body, which provided zoom-out and -in ranging from 0.63× up to 6.3×. Light sheet images were generated with different magnification factors and a step size of 5-10 µm according to sample size with 470±30 / 640±30 nm ex/em bandpass filters for QDs. Lung tissue autofluorescence was generally scanned with 520±40 / 585±40 nm ex/em filters to show the microstructure of the lungs. An exposure time of 100ms and a laser power of 95% are usually applied to LSFM, where the light sheet has different xy width and numerical aperture (NA) to suit the sample size. During the LSFM image acquisition, the sample was immersed in the DBE. Imaris 9.1.0 (Bitplane, Belfast, United Kingdom) was used to perform 2D and 3D rendering and image processing.

3.6.3 Immunoblot

3.6.3.1 Protein extraction from cell culture

Cells cultured in standard cell culture dishes were washed twice with sterile PBS and then digested in 200 µL of RIPA buffer (per well in a 6-well plate) supplemented with protease and phosphatase Inhibitors (10311494, Fisher Scientific) with the help of cell scratcher. The collected cell lysates were then transferred to Eppendorf tubes placed on ice and incubated for 45min and centrifuged at 15,000 RPM for 15min at 4°C to separate the supernatant (total protein) and the pellet (cell debris). The supernatant was transferred to a new Eppendorf and stored at -80°C for future analysis.

3.6.3.2 Nuclear and cytoplasmic protein extraction

Nuclear and cytoplasmic protein was extracted from MLE12 cells according to the manufacturer's instructions (Thermo Scientific, 78835). In brief, cells were harvested with trypsin-EDTA and then centrifuged at 500 × *g* for 5 min, washed cells by suspending the cell pellet with PBS and centrifuged again to collect the pallet. The pallet was mixed resuspended with cytoplasmic extraction reagent I and incubated on ice for 10 min, then cytoplasmic extraction reagent II for 1 min incubation on ice, and centrifuged to harvest the cytoplasmic proteins in the supernatant. The pallet was resuspended again with nuclear extraction reagent and incubated on ice for 40 min, and centrifuged to harvest the nuclear proteins in the supernatant.

3.6.3.3 Protein extraction from lung tissue

Frozen lung tissue of approximately 30 mg were placed in Eppendorf tubes with 600 µL of RIPA lysis buffer containing protease and phosphatase Inhibitors. The lung tissue was homogenized by dismembrator (IKA T10, Ultra Turrax), incubated on ice for 45min, and then centrifuged at 15,000 g for 10min at 4°C. The supernatant was transferred to a new Eppendorf and stored at -80°C for future analysis.

3.6.3.4 Protein concentration estimation by bicinichonic acid (BCA) assay

Protein concentration measurement was performed using the BCA assay (Pierce Scientific Rockford, IL, USA, 23227) according to the manufacturer's instructions. A bovine serum albumin (BSA) titration curve with a concentration range of 0-2 µg/µL diluted in RIPA buffer served as a standard to determine protein concentrations. Protein samples from cell culture were diluted at a ratio of 1:5 with RIPA

buffer and lung tissue samples with 1:10 ratio. After incubation at 37°C for 30min, the absorbance at 562 nm was recorded using a Sunrise TM plate reader (TECAN) and calculated for protein concentrations.

3.6.3.5 SDS-PAGE immunoblotting

Protein samples were diluted to the same concentration and mixed with LDS sample buffer (NP0007, NuPAGE™) and sample reducing agent (NP0009, NuPAGE™), and denatured at 90°C for 10min. A nupage electrophoresis system was employed for the blotting. Samples of 22 µg were loaded to a 4-12% Bis-Tris polyacrylamide gel (NP0336BOX, Life Technologies) alongside the protein standard (Magicmark XP, LC5602, Life Technologies). Gel electrophoresis was performed in MES running buffer for 60min at 150 V. Nitrocellulose membranes (LC2006, Life Technologies) were activated in the transfer buffer for 10min prior to protein transfer. Proteins were transferred from gel to the membrane at 30 V in transfer buffer for 60min. The membrane was blocked with 5% skim milk (70166, Sigma Aldrich) in 0,1% TBS-T for 1h at RT, and then with primary antibodies diluted in 5% milk solution at 4°C overnight. After the overnight incubation, the membrane was washed 3x10min with TBS-T and incubated with corresponding HRP-conjugated secondary antibody for 1.5h at RT, washed 3 times and developed with SuperSignal™ West Femto Maximum Sensitivity Substrate (34096, Life Technologies) and recorded with a Chemidoc XRS system (BIO-Rad). Quantification of band intensity was performed with ImageJ and normalized to the β-actin.

3.7 Histology

Four randomly selected tissue sections per animal (n=4/group) were treated with Hart's elastin stain for assessment by automated video thresholding of stain color

using the Bioquant True Color Windows Image Analysis system (R & M Biometrics, Nashville, TN). Quantification expressed positively stained elastic fibers in relation to the total lung tissue. A total of 12 HPF at 400x were assessed per animal.

3.8 Statistical analysis

Data were analyzed with GraphPad Prism 8.0(GraphPad, San Diego, CA). All statistical tests were conducted as 2-sided tests, and the level of significance was set at 5 %. Statistical analysis was performed with unpaired t-tests or One-way ANOVA with Dunnett's multiple comparison test. Results were presented as mean ± standard deviation (SD). The "n" refers to number of biological replicates included in the experiments. The statistical significance is stated in the figure legends in the results section.

4. Results

4.1 ERBB3 signaling in last stage developing lung

4.1.1 Temporal and spatial resolution of pERBB3 level correlates with the postnatal alveolarization process

In the neonatal mouse lung, postnatal development is realized by the orchestration of the distal epithelium, endothelium, and fibroblasts through secondary septation, resulting in the expansion of surface area for gas exchange (**Fig 6 a-g**).

In lung slide from healthy termed-born mice, quantification results from IHC staining showed that the phosphorylated ERBB3 receptor levels peaked on PND 5 (**Fig 6 h**) in lung periphery and remained at that high level until PND14, corresponding to the phase of postnatal alveolarization. Our preliminary studies revealed that the Platelet-derived growth factor subunit A (PDGF-A) expression peaked at PND5, followed by sustained increase in its receptor PDGF-Rα expression until PND 14.

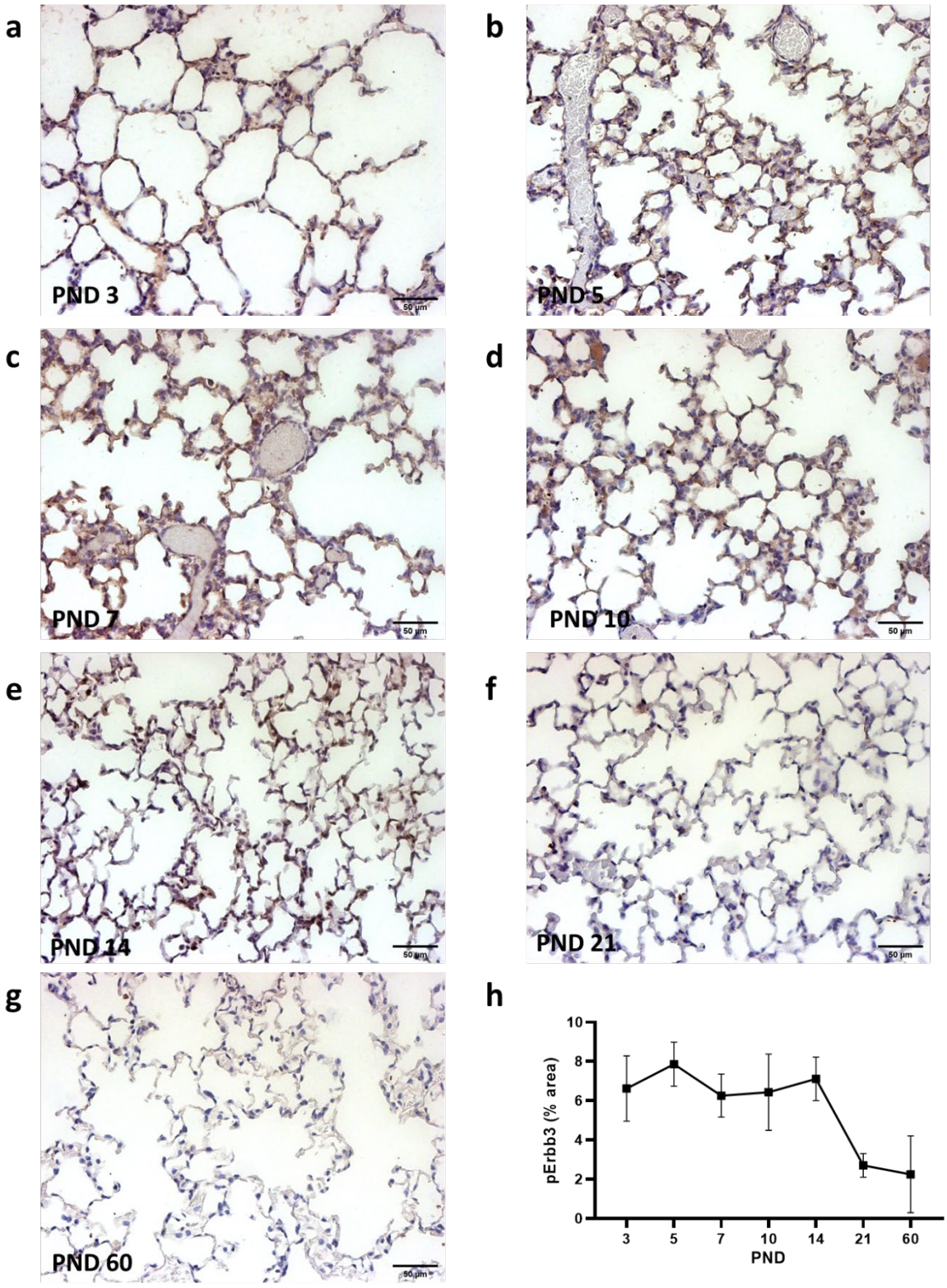

Fig 6. Immunohistochemistry staining of phosphorylated Erbb3 in neonatal mouse lung section, **a-g**) PND 3, 5, 7, 10, 14, 21, and 60, counterstained with hematoxylin, 200X magnification. **h)** quantification of pErbb3 stained in peripheral lung tissue, expressed as percentage of positive tissue area.

4.1.2 Cell specific expression of ERBB3

Single cell RNA sequencing data from our collaborative studies(Negretti et al. 2021) revealed that Erbb3 is predominantly expressed in type 1, 2 alveolar epithelial cells (AEC1, AEC2), ciliated cells, as well as neuron cells postnatally (**Fig 7 a**). The ligand (NRG1) for the ERBB3 receptor is expressed in AEC1, ciliated cells, and matrix fibroblasts postnatally, and also in venous endothelial cells showing a decreased expression from E12 to P14(**Fig 7 b**). Other ligands like PDGF-A and VEGF-A are also primarily expressed in the AEC1 cells from E15 to P14 during the saccular and alveolarization stages. They are secreted into the extracellular environment and bind receptors on PDGF-Rα positive fibroblasts and ECs via paracrine (**Fig 7 c, d**)(Negretti et al. 2021).

We also analyzed the pre- and postnatal expression of other ERBB receptors in this dataset. The ERBB2 expression seemed to be universal in most epithelial and mesenchymal cell types, while ERBB4 was only mildly expressed in mesothelium and smooth muscle cells **(Fig 7 e, f)**.

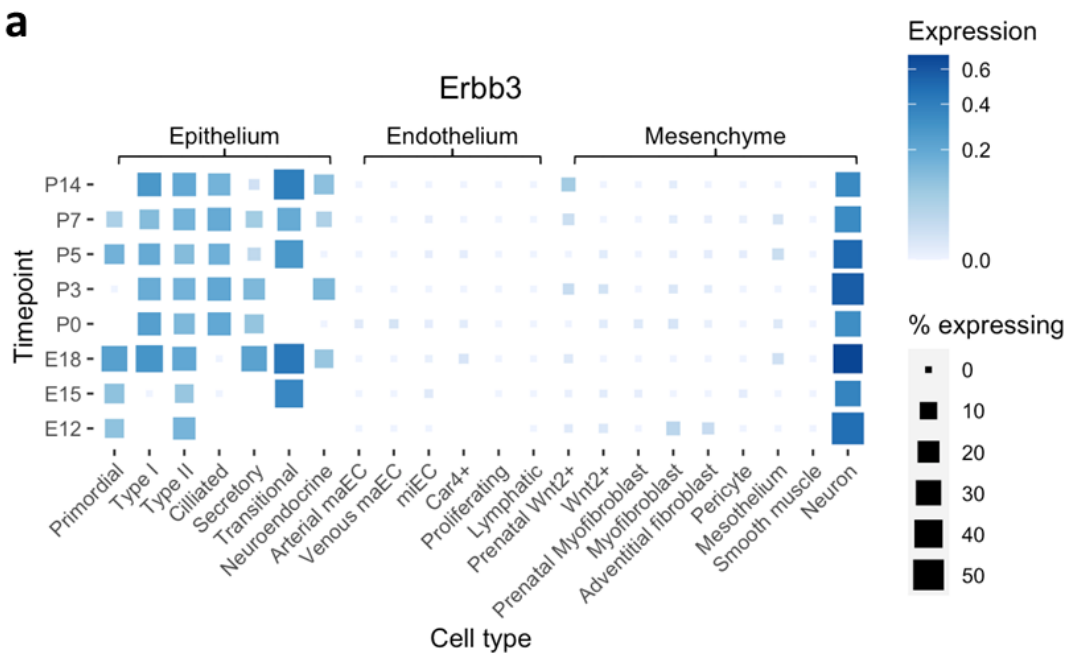
a
Erbb3
Epithelium
Endothelium
Mesenchyme
Timepoint
P14
P7
P5
P3
P0
E18
E15
E12
Primordial
Type I
Type II
Ciliated
Secretory
Transitional
Neuroendocrine
Arterial maEC
Venous maEC
miEC
Car4+
Proliferating
Lymphatic
Prenatal Wnt2+
Wnt2+
Prenatal Myofibroblast
Myofibroblast
Adventitial fibroblast
Pericyte
Mesothelium
Smooth muscle
Neuron
Cell type
Expression
0.6
0.4
0.2
0.0
% expressing
0
10
20
30
40
50

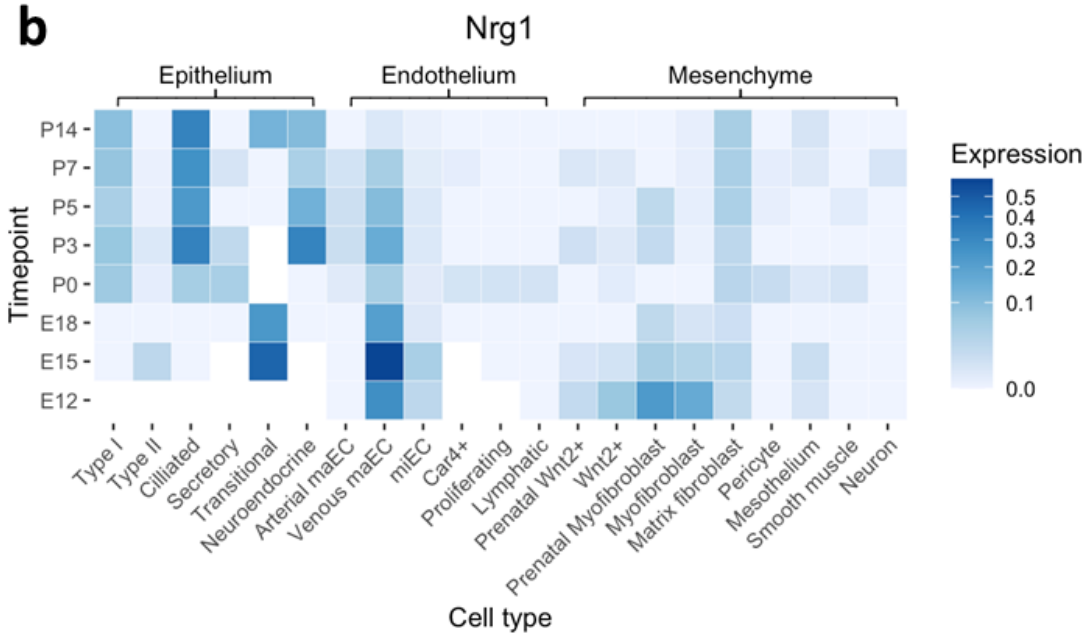
b
Nrg1
Epithelium
Endothelium
Mesenchyme
Timepoint
P14
P7
P5
P3
P0
E18
E15
E12
Type I
Type II
Ciliated
Secretory
Transitional
Neuroendocrine
Arterial maEC
Venous maEC
miEC
Car4+
Proliferating
Lymphatic
Prenatal Wnt2+
Wnt2+
Prenatal Myofibroblast
Myofibroblast
Matrix fibroblast
Pericyte
Mesothelium
Smooth muscle
Neuron
Cell type
Expression
0.5
0.4
0.3
0.2
0.1
0.0

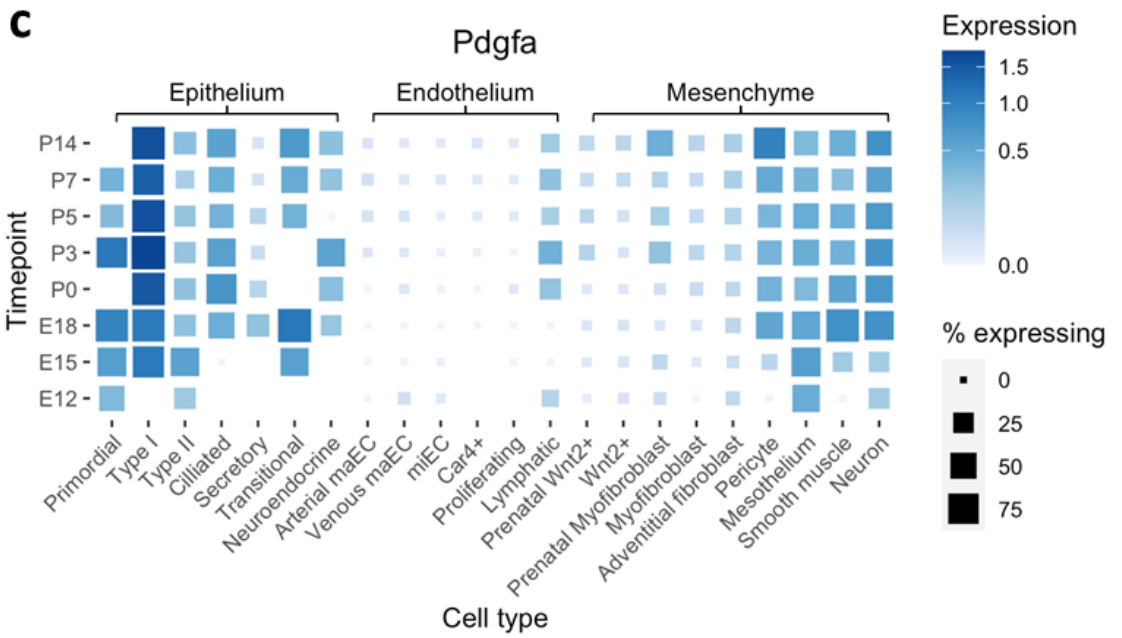
c
Pdgfa
Epithelium
Endothelium
Mesenchyme
Timepoint
P14
P7
P5
P3
P0
E18
E15
E12
Primordial
Type I
Type II
Ciliated
Secretory
Transitional
Neuroendocrine
Arterial maEC
Venous maEC
miEC
Car4+
Proliferating
Lymphatic
Prenatal Wnt2+
Wnt2+
Prenatal Myofibroblast
Myofibroblast
Adventitial fibroblast
Pericyte
Mesothelium
Smooth muscle
Neuron
Cell type
Expression
1.5
1.0
0.5
0.0
% expressing
0
25
50
75

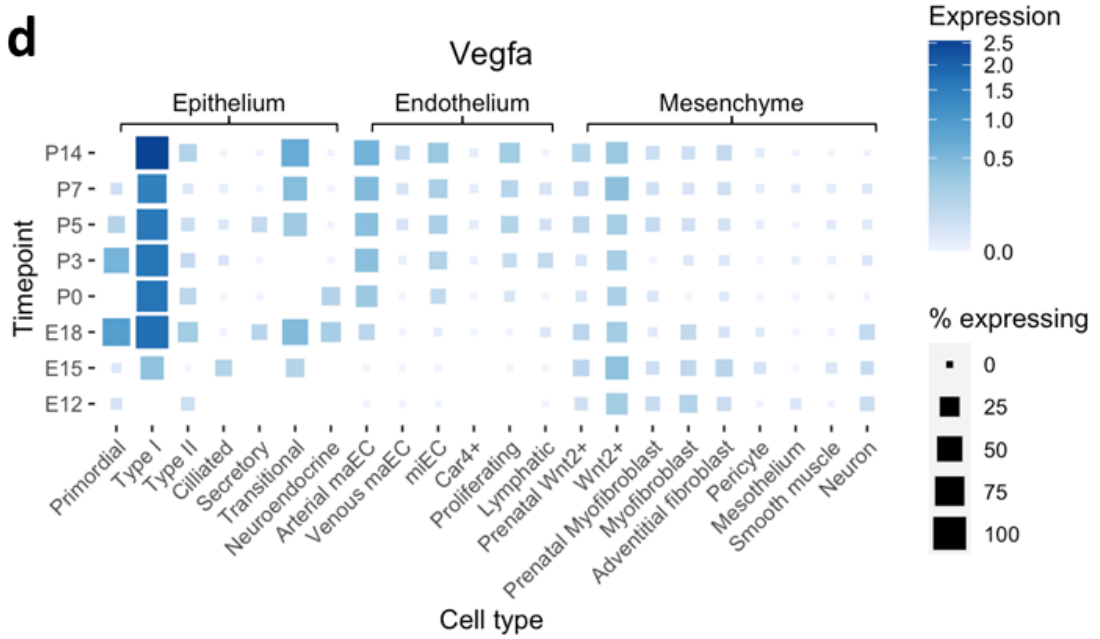
d
Vegfa
Epithelium
Endothelium
Mesenchyme
Timepoint
P14
P7
P5
P3
P0
E18
E15
E12
Primordial
Type I
Type II
Ciliated
Secretory
Transitional
Neuroendocrine
Arterial maEC
Venous maEC
miEC
Car4+
Proliferating
Lymphatic
Prenatal Wnt2+
Wnt2+
Prenatal Myofibroblast
Myofibroblast
Adventitial fibroblast
Pericyte
Mesothelium
Smooth muscle
Neuron
Cell type
Expression
2.5
2.0
1.5
1.0
0.5
0.0
% expressing
0
25
50
75
100

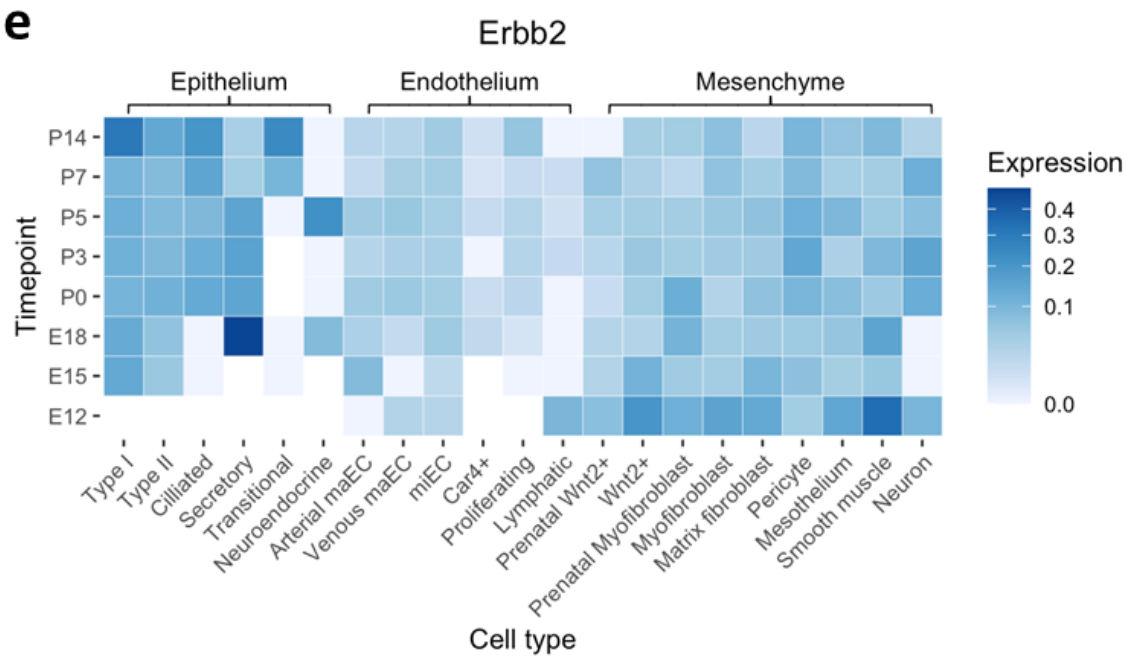
e
Erbb2
Epithelium
Endothelium
Mesenchyme
Timepoint
P14
P7
P5
P3
P0
E18
E15
E12
Type I
Type II
Ciliated
Secretory
Transitional
Neuroendocrine
Arterial maEC
Venous maEC
miEC
Car4+
Proliferating
Lymphatic
Prenatal Wnt2+
Wnt2+
Prenatal Myofibroblast
Myofibroblast
Matrix fibroblast
Pericyte
Mesothelium
Smooth muscle
Neuron
Cell type
Expression
0.4
0.3
0.2
0.1
0.0

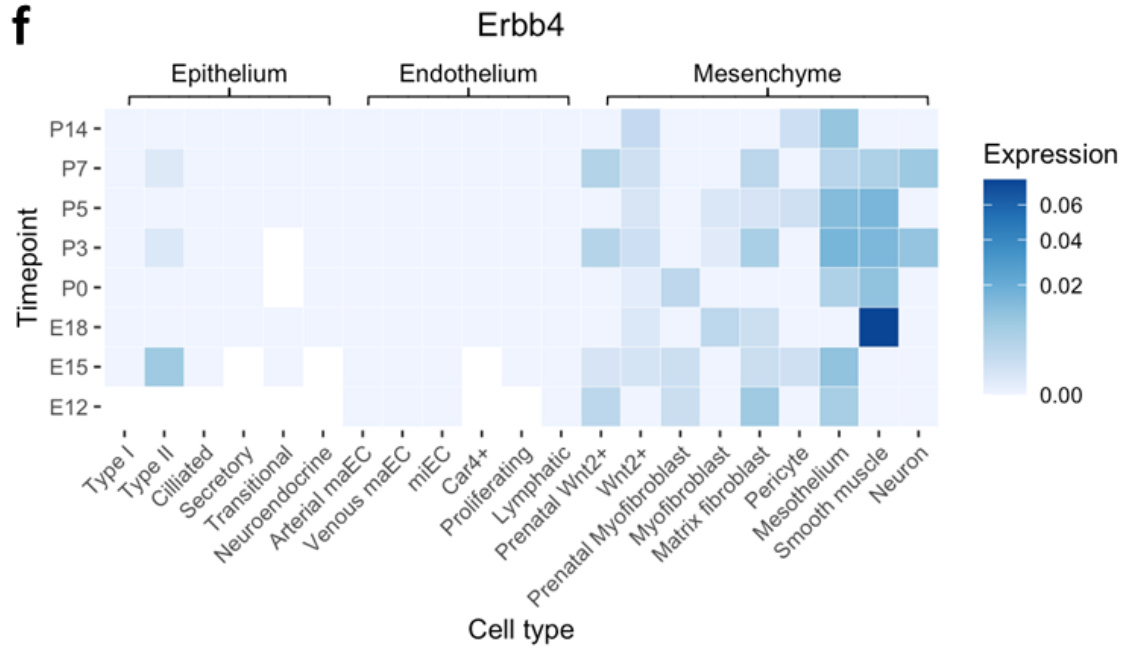
f
Erbb4
Epithelium
Endothelium
Mesenchyme
Timepoint
P14
P7
P5
P3
P0
E18
E15
E12
Type I
Type II
Ciliated
Secretory
Transitional
Neuroendocrine
Arterial maEC
Venous maEC
miEC
Car4+
Proliferating
Lymphatic
Prenatal Wnt2+
Wnt2+
Prenatal Myofibroblast
Myofibroblast
Matrix fibroblast
Pericyte
Mesothelium
Smooth muscle
Neuron
Cell type
Expression
0.06
0.04
0.02
0.00

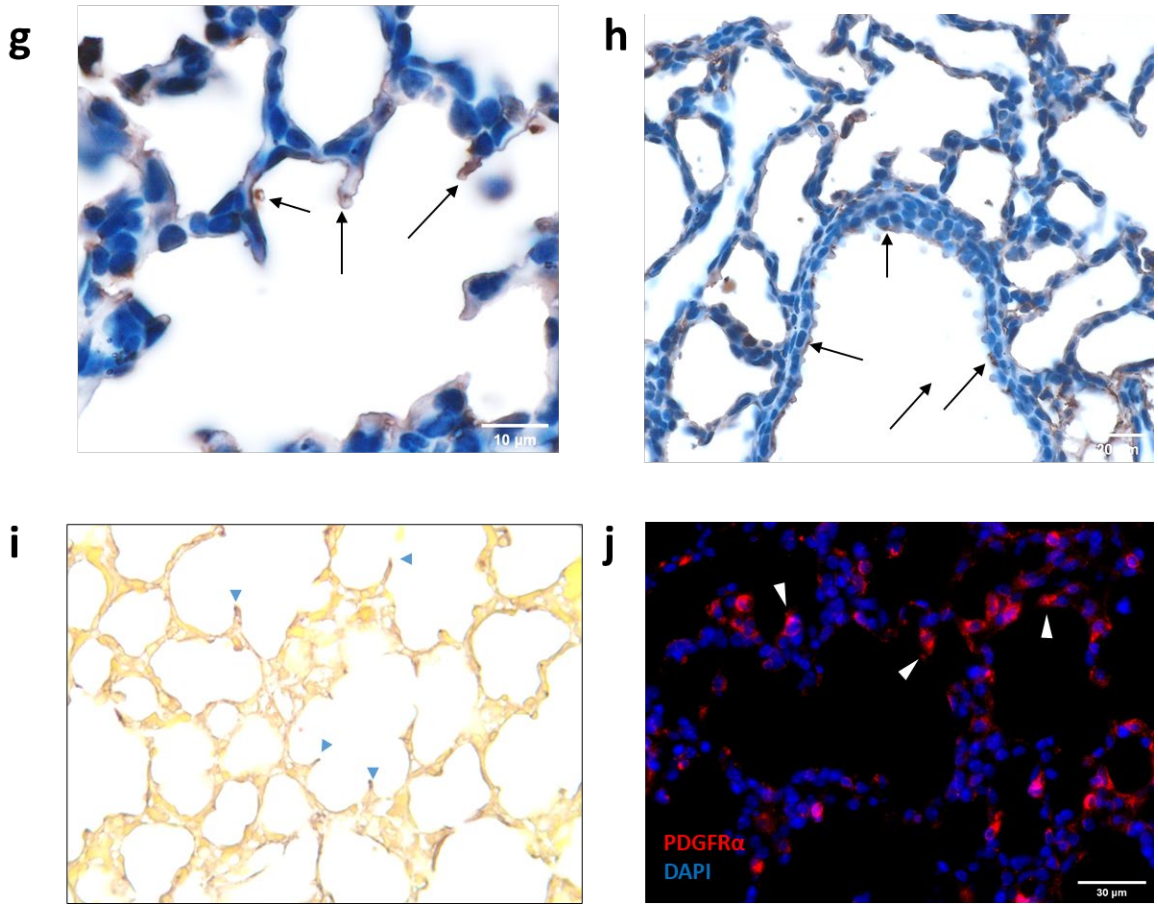

Fig 7. Single cell RNA sequencing analysis of different gene expression obtained from pre- and postnatal mouse lung cells; **a)** *Erbb3*; **b)** *Nrg1*; **c)** *Pdgfa*; **d)** *Vegfa*; **e)** *Erbb2*; **f)** *Erbb4*; **g)** Immunohistochemistry staining of pERBB3 in neonatal C57BL/6J mouse (PND7) lung peripheral section, counterstained with hematoxylin, 1000X, black arrow: ERBB3 phosphorylation at the septal tip; **h)** pERBB3 in terminal bronchial epithelial cells, 400X, black arrow: ciliated cells; **i)** Elastin staining of neonatal lung peripheral at PND 7, arrow: Elastin; **j)** immunofluorescent staining of PDGF-Rα in neonatal lung peripheral at PND 7, arrow: PDGF-Rα.

4.1.3 Localization of ERBB3 at septal tips

As scRNA sequencing results indicated the temporal correlation of ERBB expression with the postnatal alveolarization process, we then proceeded to the localization of ERBB3 in the periphery of mouse developing lung. In mouse lung at PND7, phosphorylated ERBB3 was located on the membrane of alveolar epithelium, and particularly at the septal tips **(Fig 7 g).** Elastin and PDGF-Rα positive

myofibroblasts are proven essential in the initiation of secondary septation. They are co-localized with ERBB3 at the septal tips (**Fig 7 i, j**). The ERBB3 was also concentrated at the terminal airway epithelium, presumably in ciliated cells as the scRNA sequencing data suggested (**Fig 7 h**).

It is known that at cellular level the coordinated growth of secondary septae is initiated by the migration of PDGF-Rα positive myofibroblasts to the septal tips following the gradient of PDGF-A excretion by the AEC2 cells (Gouveia, Betsholtz, and Andrae 2018), followed by the deposition of Elastin and collagen, which provide the scaffold for the septa to further elongate and divided the air space.

However, the underlying epithelial-mesenchymal crosstalk via central growth factor signaling pathways that mediate septation remained largely unexplored. Our next step aimed at unraveling the ERBB3 related pathway regulation and crosstalk during this process.

4.2 Interplay of fibroblast and epithelial cells in *ex vivo* neonatal lung organoids

4.2.1 *Ex vivo* organoid model of the developing lung

We employed an *ex vivo* model of alveolar cell-derived organoids (**Fig 8 a**), that can recapitulate lung architectural and functional changes during lung development, to further investigate the interplay between epithelial cells and fibroblasts. Primary mouse epithelial cells (PMEC) were isolated from both neonatal (PND 7) and adult female (12-week-old) mouse lungs, and co-cultured with fibroblast cell line (Mlg). This model allowed us to observe the morphological changes in the

organoids co-cultured from mesenchymal and parenchymal cells, and also evaluate the effect of pathway modulation on the organoid formation.

The co-culture of PMEC and Mlg cells formed round organoids with/without lumen after 7 days of culture, and the organoids significantly expanded in size after 14 days of culture (**Fig 8 g, h**). Immunofluorescent staining showed that those organoids comprised different epithelial cell types, including AEC1 ($HOPX^+$), AEC2 ($SP\text{-}C^+$), ciliated cells ($ac\text{-}Tubulin^+$), basal cells ($KRT5^+$) as well as PDGF-Rα positive myofibroblasts (**Fig 8 b-d, f**).

Each organoid was developed from a small cell cluster that centered by PDGF-Rα positive myofibroblasts and then epithelial cells from alveolar or airway were recruited to the PDGF-Rα positive myofibroblasts and built the wall of organoids in a thin lining similar as the alveolar and airway epithelium. Alpha-SMA protein was distributed along the inner surface of the organoid to provide structural support for the 3D morphology (**Fig 8 e**).

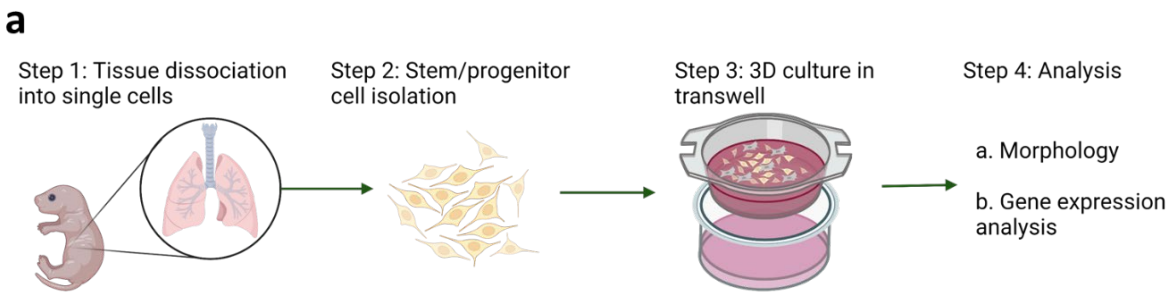

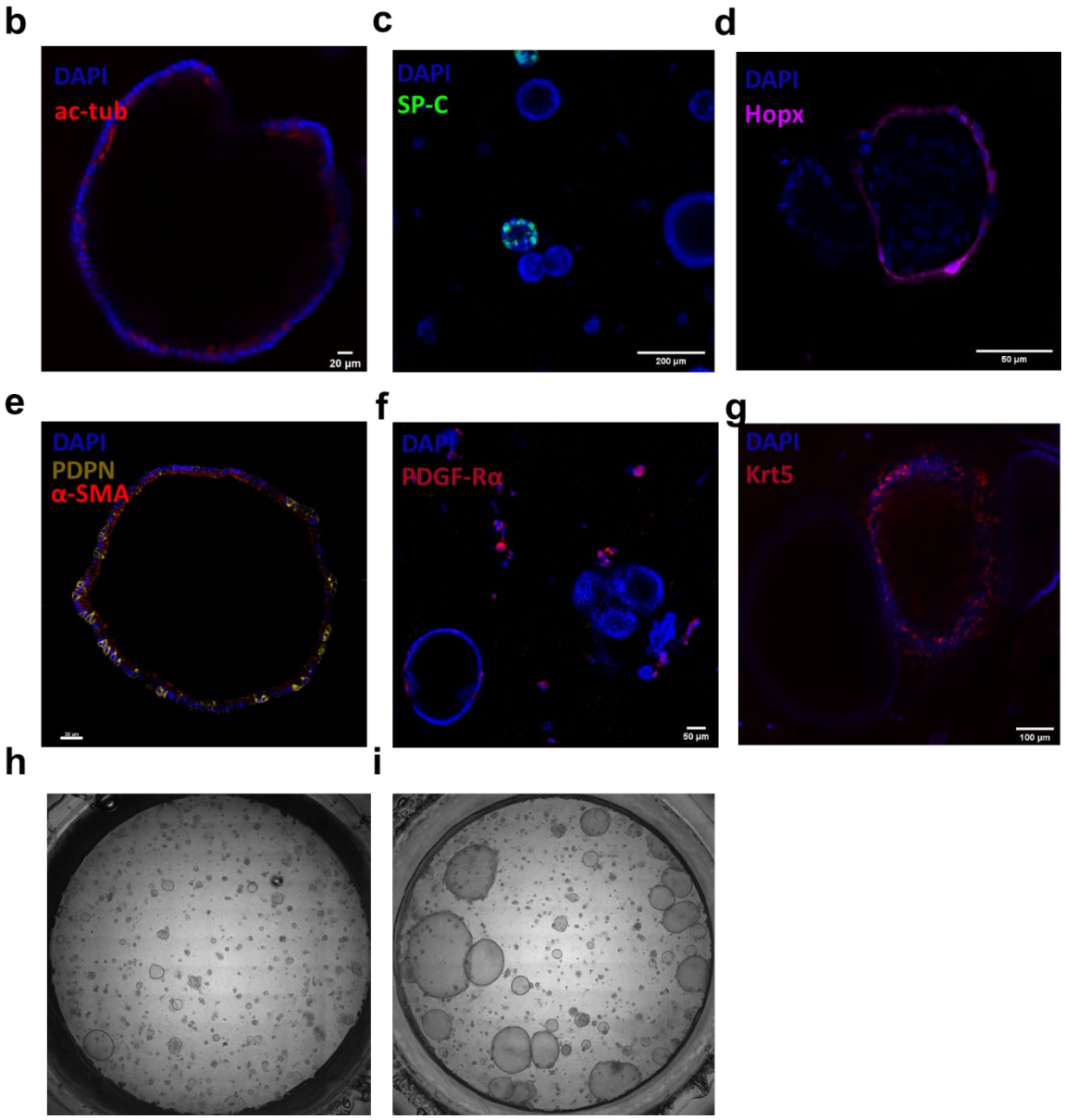

Fig 8. a) Schematic of *ex vivo* lung organoids model; **b)** Immunofluorescent staining of ciliated cells by ac-tubulin in lung organoids derived from neonatal PMEC and Mlg cells; **c)** Immunofluorescent staining of AEC2 cells by SP-C; **d)** Immunofluorescent staining of AEC1 cells by Hopx; **e)** Immunofluorescent staining of α-SMA in organoids composed of AEC1 cells (PDPN); **f)** Immunofluorescent staining of fibroblasts by PDGF-Rα; **g)** Immunofluorescent staining of basal cells by KRT5; **h)** Phase-contrast image of neonatal organoids derived after 7 days of culture; **i)** Phase-contrast image of organoids derived after 14 days of culture.

4.2.2 Activated Erbb3 signaling promotes the organoids growth

In order to further investigate the role of ERBB3 in the PMEC-fibroblasts derived organoids, we treated the organoids with supplemental ERBB3 ligand (NRG1, 8 and 80 ng/mL) after the first week of culture for another 7 days. The NRG1 was diluted in the culture medium and refreshed every other day together with the medium change. After the NRG1 treatment we demonstrated a dose-related effect in organoid morphology (**Fig 9 a**). The organoids treated with NRG1 were more segmented and had increased Ferret's diameter (**Fig 9 c**), indicating that the activation of ERBB3 pathway stimulates the organoids' expansion, but did not alter the colony forming efficiency (**Fig 9 b**). Quantitative PCR revealed upregulation of ERBB3 in the organoids upon NRG1 treatment without statistical significance (**Fig 9 f**), but no change in PDGF-Rα expression level (**Fig 9 e**). This is potentially due to the fact that the mRNA was harvested from a mixture of fibroblasts and differentiated epithelial cells, the potential effect in the receptor regulation might have been disguised by other cells that doesn't express ERBB3. In the NRG1 treated organoids, HOPX expression level normalized by the nuclear stain (DAPI) was increased comparing to the control group, suggesting an increased number of AEC1 cells in the organoids (**Fig 9 d**).

a

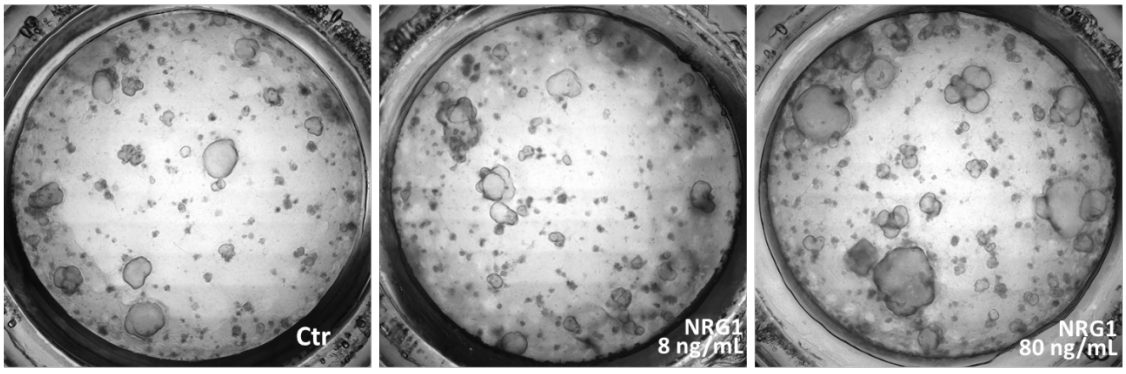

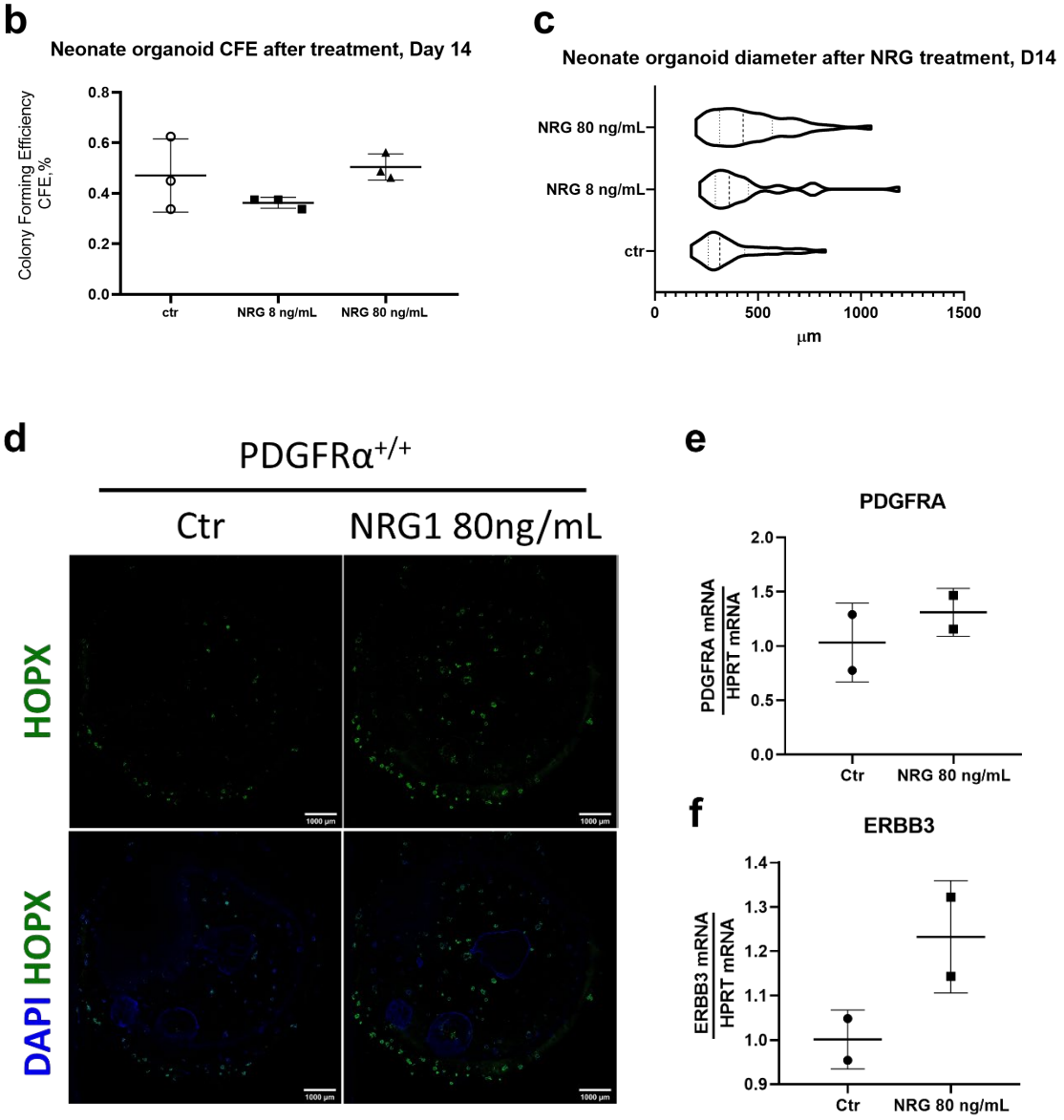

Fig 9. a.) Phase-contrast image of organoids derived after 7 days of culture + 7 days of NRG1 treatment, projected image, 100X, BF, left: control; middle: NRG1 8 ng/mL; right: NRG1 8 ng/mL; **b)** Colony forming efficiency of organoids after 14 days of culture, mean ± SD; **c)** combined quantification results of Ferret's diameter in organoids after NRG1 treatment, n=3; **d)** Immunofluorescent staining of HOPX in lung organoids derived from primary fibroblasts and PMEC, 100X; left column: control, right column: NRG1 treatment (80 ng/mL); **e)** mRNA level of Pdgfra in organoids treated with NRG1; **f)** mRNA level of *Erbb3* in organoids treated with NRG1, mean ± SD. t-test, n=3.

4.2.3 Distinct morphological characteristics of neonatal lung organoids

Then we focused on the impact of myofibroblasts on the organoid formation. Before seeding the PMECs together with the fibroblasts, we analyzed gene expression of PDGF-A the PMECs by qPCR. The PDGF-A expression level in isolated neonatal PMECs was 3.9 folds higher as compared to adult PMECs. After 7 days of culture, PDGF-A expression in neonatal organoids was significantly higher than in adult organoids (**Fig 10 a-c**). After 14 days of culture, organoids derived from neonatal primary epithelial cells ($CD45^-/CD31^-$) revealed distinct characteristics when compared to organoids derived from adult epithelial cells (**Fig 10 e, f**). While the adult organoids had two major clusters with a calculated Ferret's diameter around 150 µm and 300 µm, the neonatal organoids were close to 450 µm in diameter (**Fig 10 g**). The neonatal organoids covered a broader range of size but lower colony forming efficiency (CFE) (**Fig 10 d**). These results suggest that PDGF pathway activation contributes to the expansion of organoids, but not in the development of new organoids.

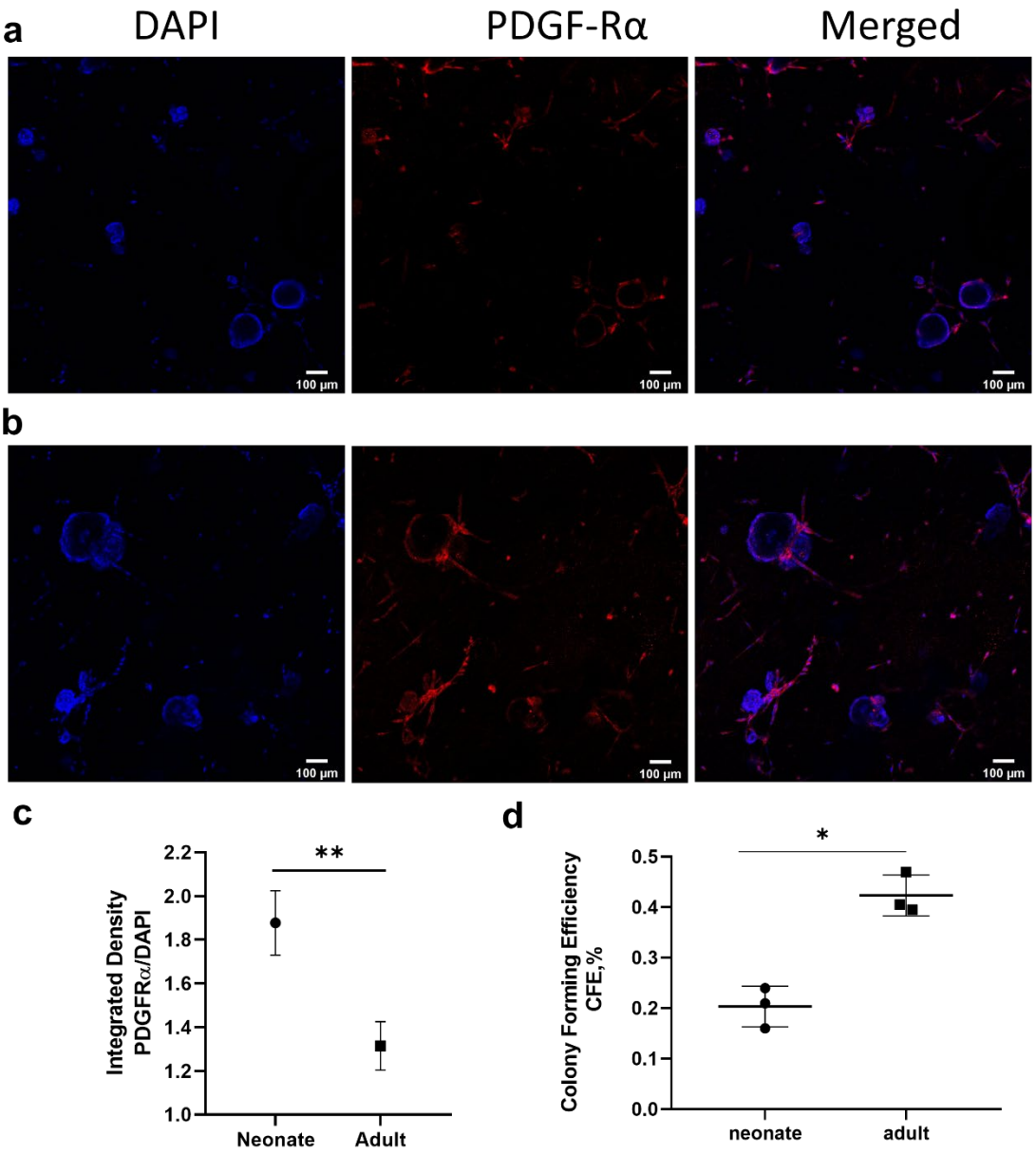
a
DAPI
PDGF-Rα
Merged
100 µm
b
c
Integrated Density PDGFRα/DAPI
2.2
2.0
1.8
1.6
1.4
1.2
1.0
**
Neonate
Adult
d
Colony Forming Efficiency CFE,%
0.5
0.4
0.3
0.2
0.1
0.0
*
neonate
adult

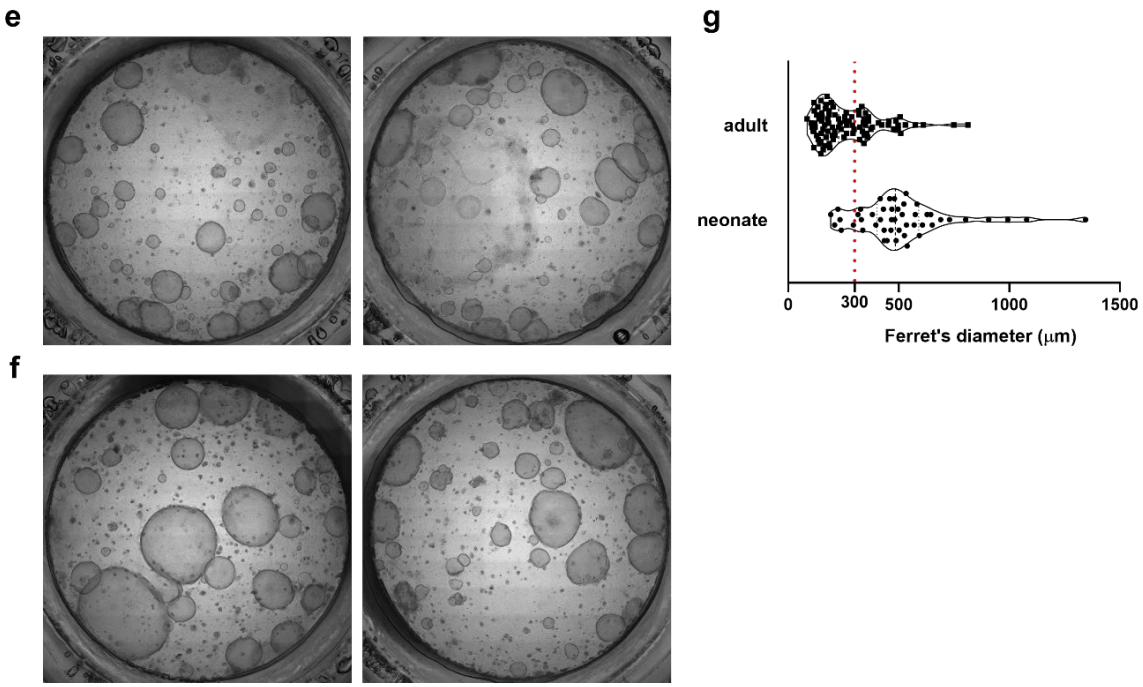

Fig 10. Immunofluorescent staining of PDGF-Rα in lung organoids derived from primary mouse epithelial cells isolated from **a)** adults mouse lung (12-week-old), **b)** neonatal mouse lung (PND 7) in co-culture with Mlg cells, blue: DAPI red: PDGF-Rα; **c)** quantification of PDGF-Rα expression level as determined by fluorescence density normalized by DAPI; phase contrast image of organoids derived from neonatal PMEC and Mlg at different ratio, mean ± SD, t test, **p<0.01, n=3/4; **d.)** Colony forming efficiency of adult organoids versus neonatal organoids, t test, n=3; **e.)** Organoids derived from co-culture of primary epithelial cells extracted from adult mouse (12-week, female) and Mlg cell line, projected image, 100X, BF; **f.)** Organoids derived from co-culture of primary epithelial cells extracted from neonatal mouse (7-day, female) and Mlg cell line, projected image, 100X, BF; **g.)** combined quantification results of Ferret's diameter in organoids, adult vs neonates, n=3.

4.2.4 PDGF-Rα positive fibroblasts contribute to the formation and segmentation of neonatal organoids

Next, we used different ratios of PMEC:Mlg cell number to see the impact of fibroblast number on organoid formation. When neonatal PMECs were cultured with higher numbers of fibroblasts, the formed organoids were smaller in size but more segmented (**Fig 11 a-c**), indicating the fibroblasts might work as a starting point that guide the epithelial protrusion towards the organoid lumen to subdivide

it into alveolar like structure. This drift in organoid size was less prominent in adult organoids (**Fig 11 d**). However, higher numbers of fibroblasts provoked more organoids with the adult primary cells (**Fig 11 f**).

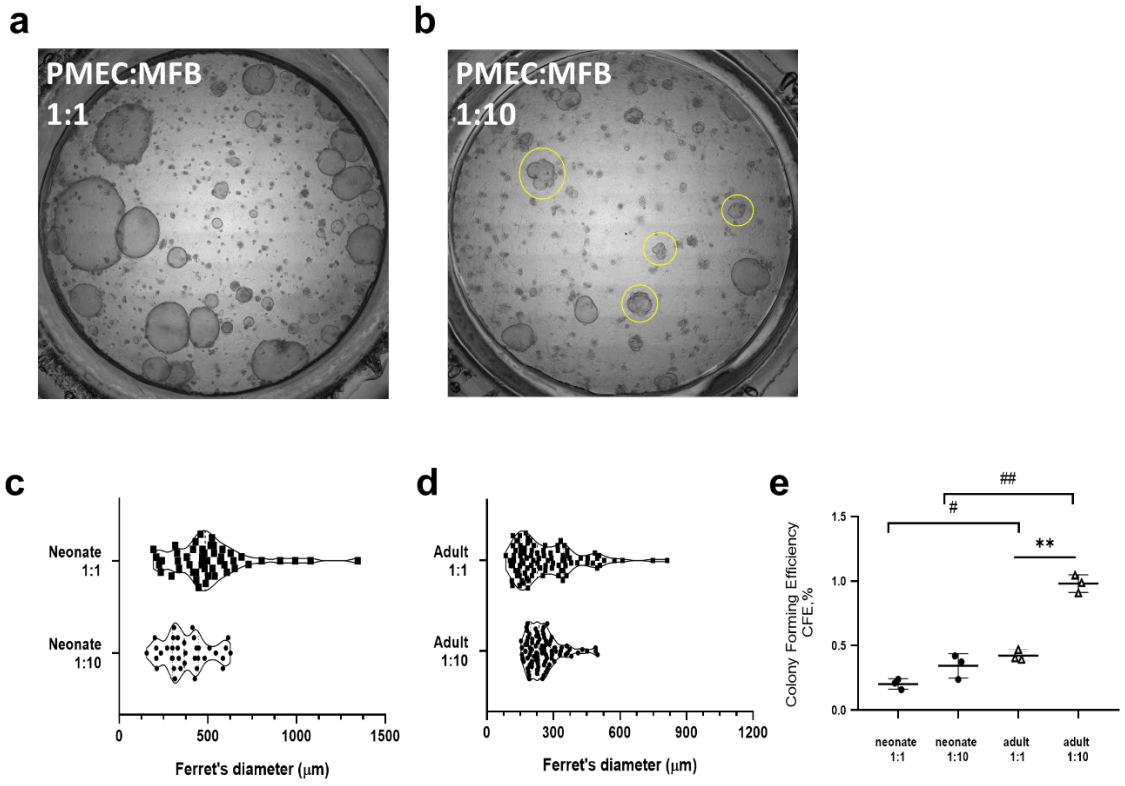

Fig 11. a) PMEC: MFB at 1:1, **b)** PMEC: MFB 1:10, bright field, 100X; **c)** combined quantification results of Ferret's diameter in neonatal organoids with different PMEC:MFB ratio; **d)** combined quantification results of Ferret's diameter in adult organoids with different PMECs: MFBs ratio; **e)** Colony forming efficiency of organoids derived from neonatal/adult PMECs : MFBs at different ratio, t test, *p<0.05, **p<0.01, n=3**.**

4.2.5 ERBB3 and PDGF pathway crosstalk in organoids and mouse lung

In order to investigate the crosstalk of PDGF and ERBB3 pathways underlying the interplay of fibroblast-epithelial cells, we then replaced the fibroblast cell line with primary fibroblasts extracted from the wildtype and heterozygous neonatal mice that carry a null mutation on one alle of the *PDGF-Rα* gene (PDGF-Rα$^{+/-}$). The co-culture was treated with NRG1 (8 and 80 ng/mL) as described in 2.3.3.

The fibroblasts culture was described in 2.2.2, and 77.2% of the fibroblasts were PDGF-Rα positive.

After 14 days of culture, organoids derived from neonatal PMEC and primary fibroblasts were smaller than the ones grew from Mlg cell line, potentially because the primary fibroblasts were more sensitive to the mitomycin treatment than the immortalized Mlg cells, therefore resulted in reduced viability of the fibroblasts.

In the organoids derived from both wildtype and PDGF-Rα heterozygous fibroblasts, NRG1 treatment did not alter the size or shape of organoids. However, in the heterozygous group, HOPX expression was significantly higher after the NRG1 treatment (**Fig 12 a**), suggesting a higher proliferation rate in the epithelial cells. Meanwhile the pERBB3 expression in PDGF-Rα$^{+/-}$ heterozygous mouse lung was significantly higher than in wildtype mouse (**Fig 12 b, c**). This explains the fact that ERBB pathway activation by the NRG1 treatment was more significant in heterozygous mice and led to larger increase in HOPX upregulation (**Fig 12 d**).

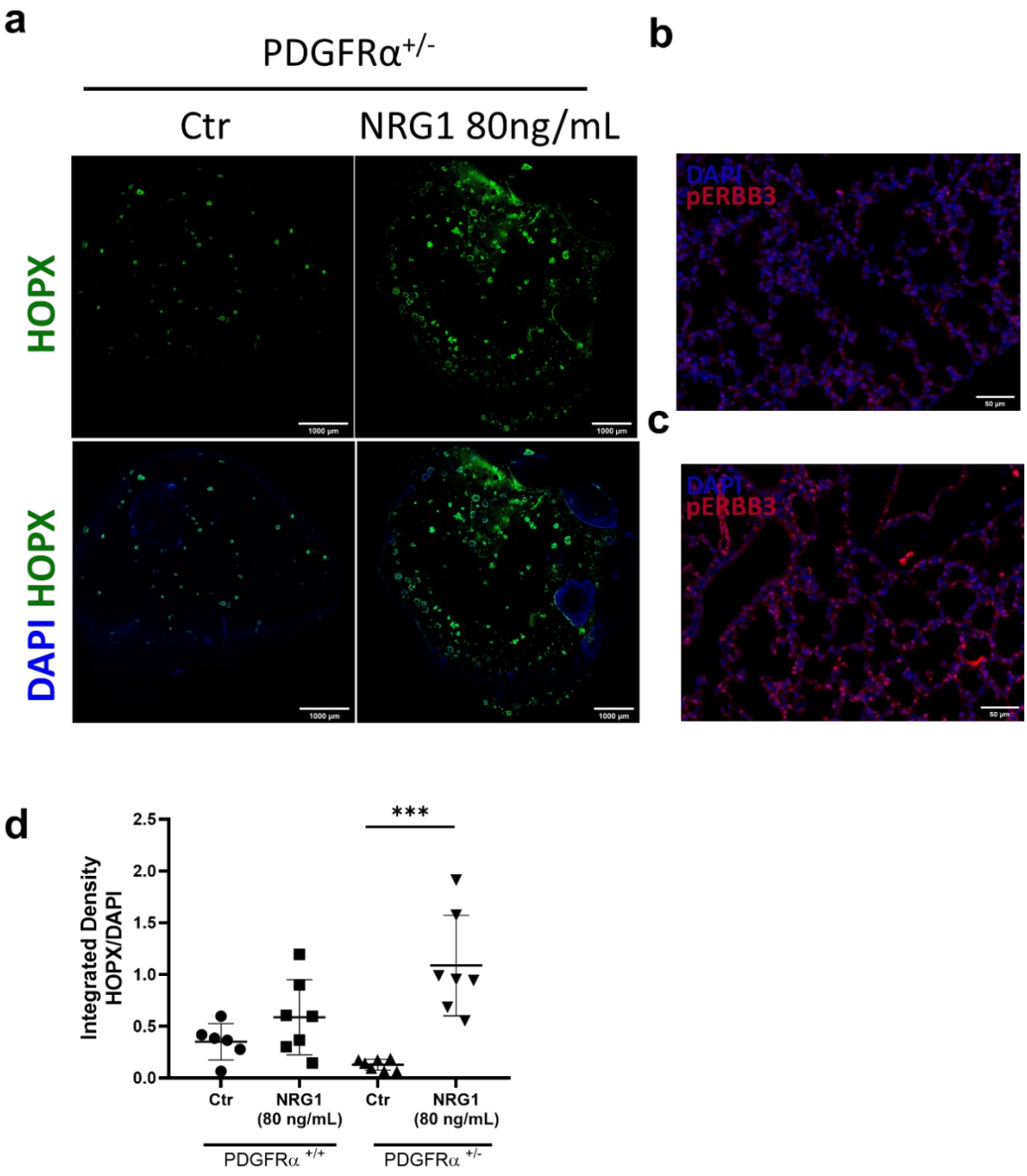

Fig 12. a) Immunofluorescent staining of HOPX in lung organoids derived from primary PDGF-Rα heterozygous fibroblasts and PMEC, 100X; left column: control, right column: NRG1 treatment (80 ng/mL); **b)** Immunofluorescent staining of phosphorylated ERBB3 (y1222) in WT neonatal mouse (PND7) lung section, 200X magnification; **c)** pERBB3 in PDGF-Rα$^{+/-}$ heterozygous mouse; **d)** quantification of HOPX expression level by integrated fluorescence density normalized by DAPI, t-test, ***p<0.0001, n=6/7.

4.2.6 ERBB3 and PDGF pathway crosstalk in *in vitro* co-culture model

Next, we used a non-contacting co-culture system to illustrate the interaction of fibroblasts and epithelial cells. Fibroblasts were seeded in the transwell and epithelial cells in the 6-well plate bottom, with a 0.4 µm pore sized membrane in between to avoid mixing of the two cell populations (**Fig 13 a**). The transwell system allows cell-cell communication through diffusible molecules.

After 24h of co-culture, ligand expression (NRG1) was upregulated in fibroblasts when the epithelial cells were present in short distance (**Fig 13 b**). Correspondingly in the epithelial cells, ERBB3 expression was upregulated, suggesting a paracrine activation of the pathway. Together with the receptor activation, gene expression of *Gata6, Hopx, Vegfa, Abca3, and Col1a1* was upregulated, whereas expression in PDGF-A, NRG1, and AQP5 remained unchanged (**Fig 13 d-j**). HOPX is known as a negative regulator of *Gata* gene expression(Yamada et al. 2018; Yin et al. 2006), and they cooperatively drive the differentiation of type II alveolar epithelial cell and maturation of airway epithelium, and activate the AEC2 cell characteristic gene expression, as seen in *Abca3* and *Col1a1* of our study. The upregulation of VEGF-A suggested further interaction with endothelial cells that lead to angiogenesis.

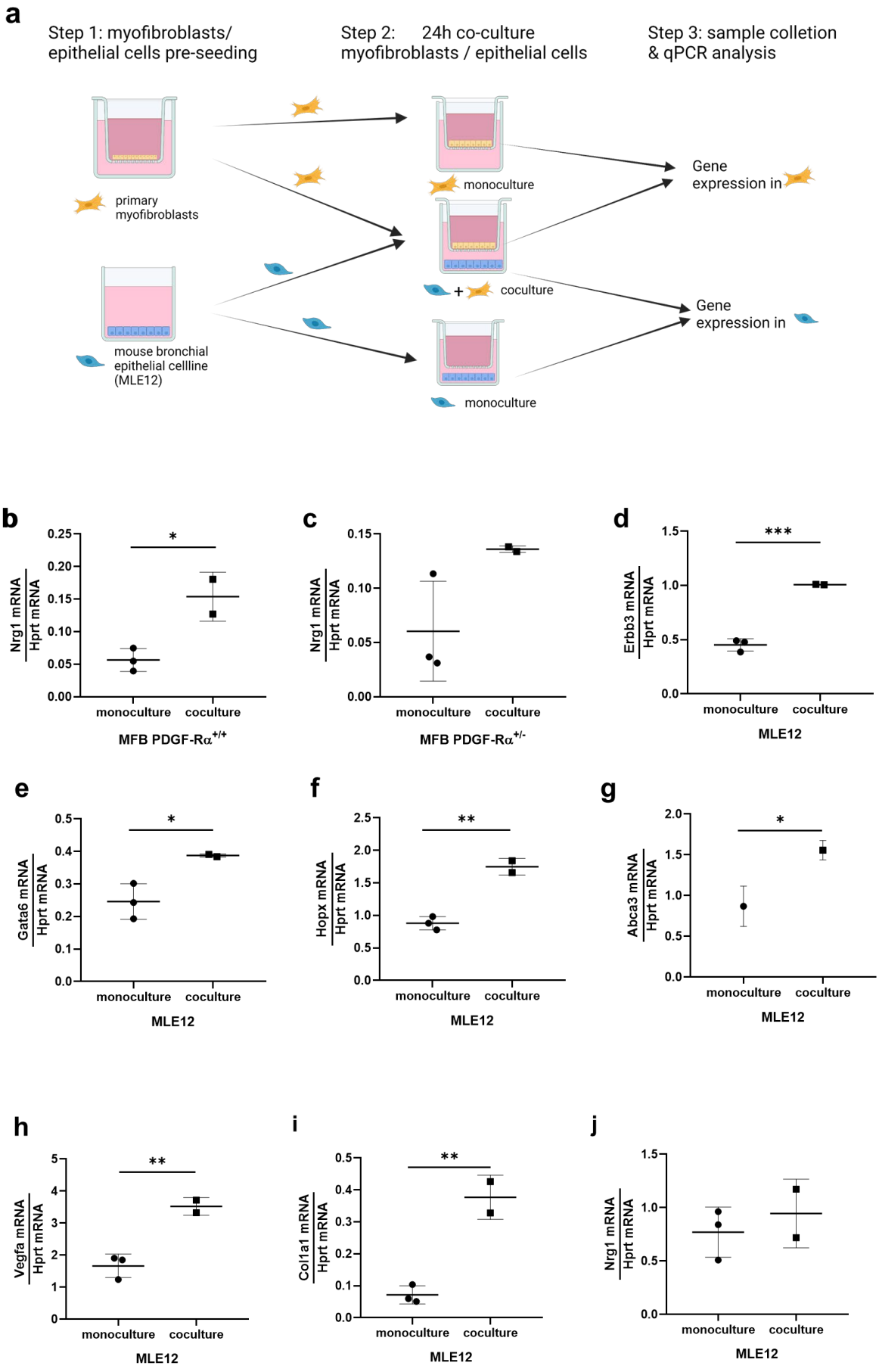
a
Step 1: myofibroblasts/ epithelial cells pre-seeding
Step 2: 24h co-culture myofibroblasts / epithelial cells
Step 3: sample colletion & qPCR analysis
primary myofibroblasts
mouse bronchial epithelial cellline (MLE12)
monoculture
coculture
monoculture
Gene expression in
Gene expression in
b
Nrg1 mRNA / Hprt mRNA
monoculture coculture
MFB PDGF-Rα+/+
c
Nrg1 mRNA / Hprt mRNA
monoculture coculture
MFB PDGF-Rα+/-
d
Erbb3 mRNA / Hprt mRNA
monoculture coculture
MLE12
e
Gata6 mRNA / Hprt mRNA
monoculture coculture
MLE12
f
Hopx mRNA / Hprt mRNA
monoculture coculture
MLE12
g
Abca3 mRNA / Hprt mRNA
monoculture coculture
MLE12
h
Vegfa mRNA / Hprt mRNA
monoculture coculture
MLE12
i
Col1a1 mRNA / Hprt mRNA
monoculture coculture
MLE12
j
Nrg1 mRNA / Hprt mRNA
monoculture coculture
MLE12

Fig 13. a) Schematic of *in vitro* lung co-culture model; **b)** mRNA level of Nrg1 in wildtype (PDGF-Rα$^{+/+}$) primary fibroblasts, t test, *p<0.05, n=2/3; **c)** mRNA level of Nrg1 in heterozygous (c) primary fibroblasts; **d-j)** mRNA level of Erbb3, Gata6, Hopx, Abca3, Vegfa, Col1a1, and Nrg1 in pathway regulation in hyperoxia injured developing lung, t test, *p<0.05, **p<0.01, ***p<0.001, n=2/3**.**

4.2.7 Decreased ERBB3 phosphorylation under hyperoxia both *in vivo* and *in vitro*

We established an *in vivo* model of neonatal lung injury to investigate the regulation of ERBB3 under hyperoxia (FiO_2=0.4) exposure. Both immunoblot and IHC staining revealed a significant decrease in phosphorylated ERBB3 in the mouse lung after 8 hours of hyperoxia exposure (**Fig 14 a, b**).

In order to further elucidate the pathway regulation at cellular level, we exposed MLE12 cells to hyperoxia for 24h and quantified ERBB3 protein separately in the nuclear and cytoplasm. Both the total and phosphorylated ERBB3 protein was more abundant in nucleus of MLE12 cells (**Fig 14 c**). Hyperoxia exposure did not alter the protein level significantly. However, phosphorylation level (pERBB3/ERBB3) was significantly higher in the nuclear than cytoplasm when the cells were cultured under room air, whereas the phosphorylation level remained at similar level for nuclear and cytoplasm of cells exposed to hyperoxia, indicating repressed nuclear translocation of ERBB3 after exposure (**Fig 14 d**). The IHC staining revealed concentrated signal of pERBB3 in MLE12 cell nuclei under room air when compared to the hyperoxia exposed cells (**Fig 14 e**). Correspondingly KI67 was also less abundant in cells exposed to hyperoxia when compared with RA, suggesting a reduced proliferation rate after exposure.

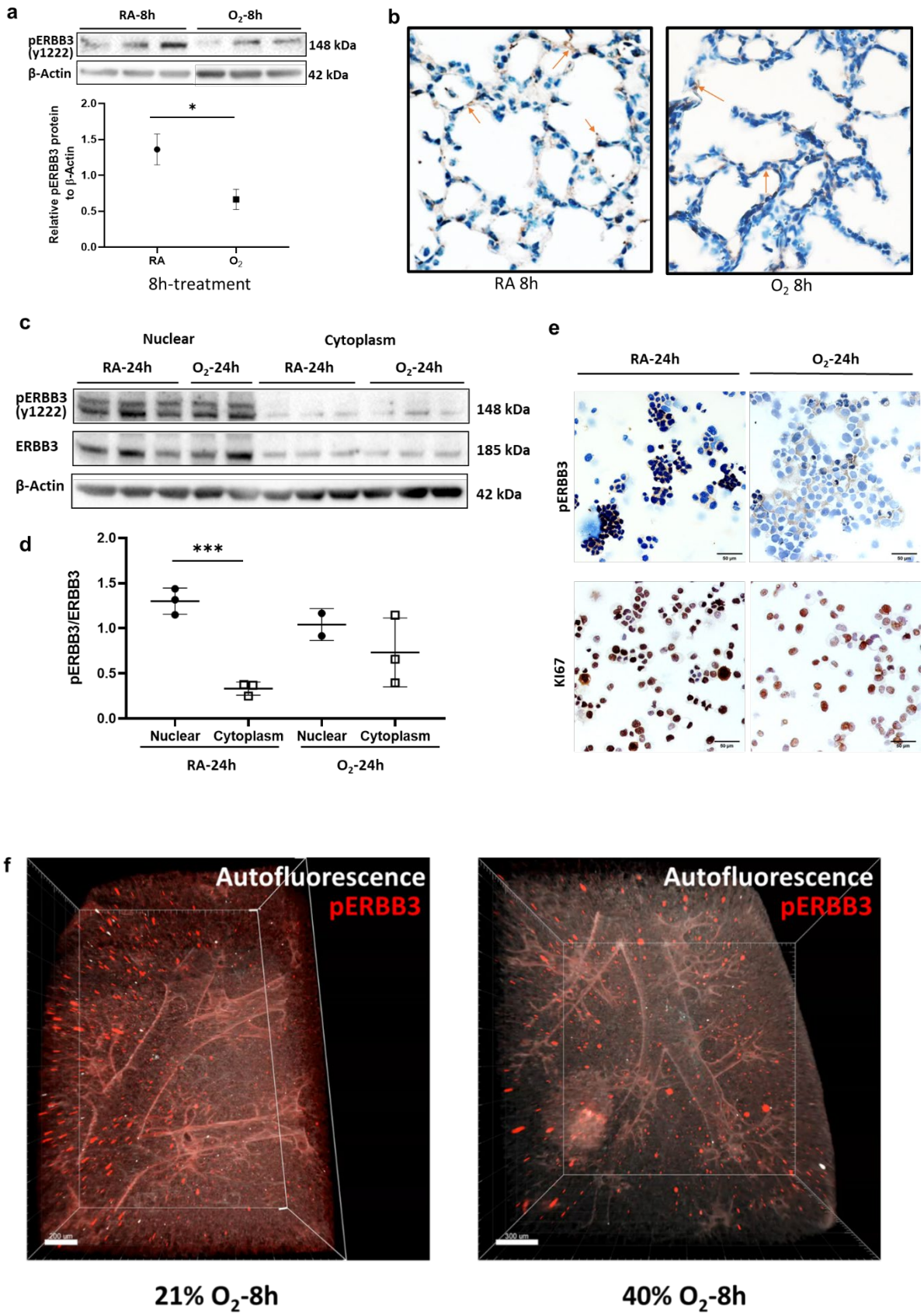

Fig 14. a) Immunoblot analysis of pERBB3 in protein lysate from neonatal mouse (PND7) lungs exposed to 8-h of hyperoxia (FiO_2=0.4), t-test, *p<0.05, n=6; **b)** Immunohistochemistry staining of phosphorylated Erbb3 (y1222) in neonatal mouse (PND7) lung section,

counterstained with hematoxylin, 200X magnification; **c)** Immunoblot analysis of pERBB3 and ERBB3 in protein lysate of MLE12 cell nuclear and cytoplasm; **d)** Quantification of ERBB3 phosphorylation (calculated by pERBB3/ERBB3, normalized by β-Actin), t test, *p<0.05, n=3; **e)** Immunohistochemistry staining of pErbb3 (y1222) (upper panel) and KI67 (lower panel) in PFA fixed MLE12 cells, counterstained with hematoxylin, 200X magnification; **f)** 3D reconstructed structure and immunofluorescent staining of pERBB3 in WT mice exposed to 8h treatment, left: RA, right: hyperoxia, light sheet microscope.

4.2.8 Compensation to hyperoxia injury weakened in PDGF-Rα$^{+/-}$ heterozygous fibroblasts

With the understanding of hyperoxia repressed ERBB3 signaling in epithelial cells, our investigation proceeded on the fibroblasts exposed to hyperoxia. In wildtype mouse primary fibroblasts exposed to 40% of oxygen for 48h, gene expression of *Pdgfra*, *Col1a1*, and *Nrg1* was significantly upregulated and Acta2 downregulated **(Fig 15 a-d)**. Proliferation level as indicated by PCNA expression was lower in hyperoxia exposed fibroblasts comparing to room air control, but the difference did not reach statistical significance **(Fig 15 e)**. Despite the upregulation of NRG1 in wildtype fibroblasts, the COLLAGEN1 and NRG1 protein level (recognized by antibody targeting the extracellular domain) did not change in response to hyperoxia exposure **(Fig 15 f, g)**. Unlike the transcriptional changes observed in wildtype fibroblasts, the upregulation of *Pdgfra* and *Nrg1* and downregulation of *Acta2* were attenuated in the PDGF-Rα$^{+/-}$ heterozygous fibroblasts and did not reach statistical significance **(Fig 15 a-d)**.

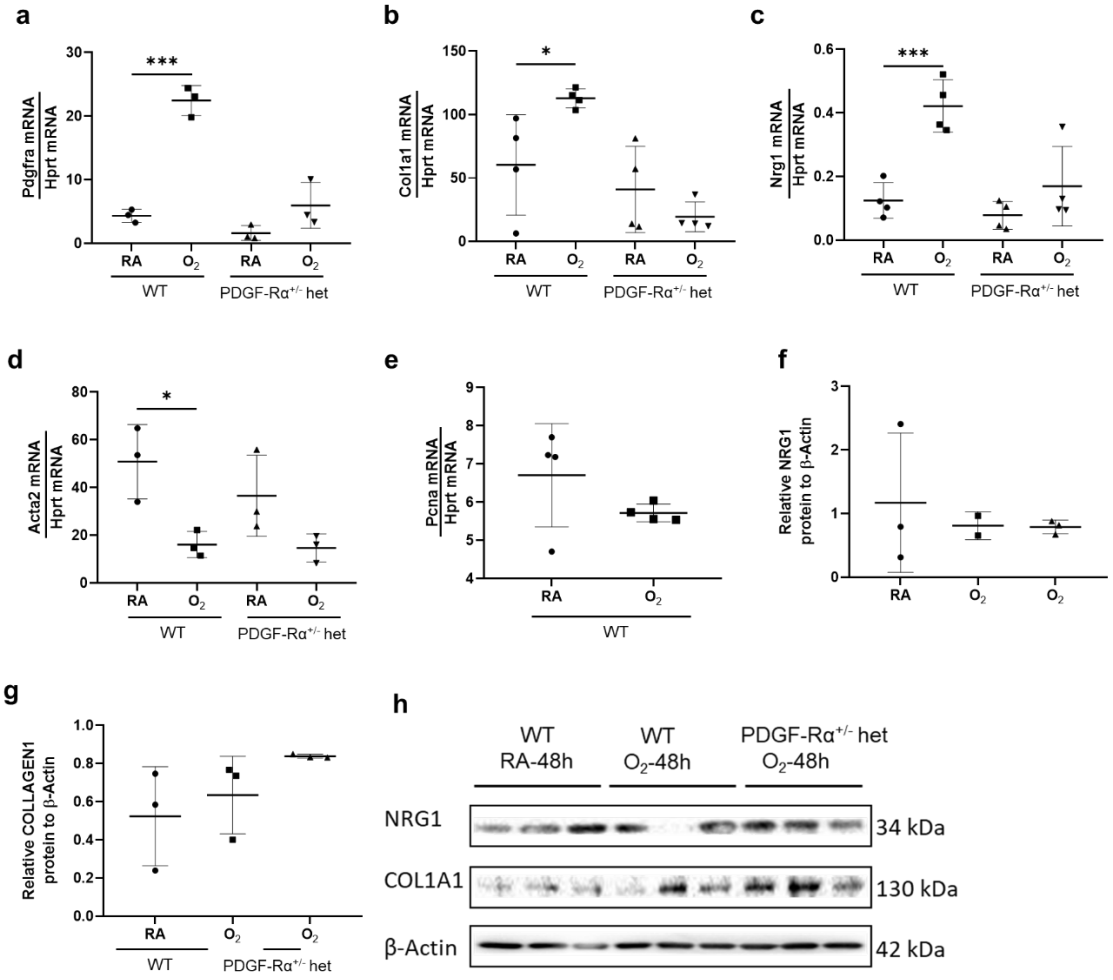

Fig 15. Gene expression level in wildtype (PDGF-Rα$^{+/+}$) and heterozygous (PDGF-Rα$^{+/-}$) primary fibroblasts exposed to 48h of 21% or 40% oxygen, one-way ANOVA with Dunnett's multiple comparison test, *p<0.05, n=3/4; **a)** *Pdgfra*; **b)** *Col1a1*; **c)** *Nrg1*; **d)** *Acta2*; **e)** *Pcna*; **f)** Immunoblot analysis of NRG1 in protein lysate from primary mouse fibroblasts exposed to 48h of 21% or 40% oxygen, one-way ANOVA, *p<0.05, n=3; **g)** Immunoblot analysis of COLLAGEN1 in protein lysate from primary mouse fibroblasts exposed to 48h of 21% or 40% oxygen, one-way ANOVA, *p<0.05, n=3; **h)** Immunoblot bands of NRG1, COLLAGEN1, and β-ACTIN in the fibroblasts lysate.

Although the hyperoxia exposure induced significant upregulation of NRG1 in fibroblasts, we did not observe any increase at protein level. Knowing that the ligand is a transmembrane protein anchored on the fibroblasts and the active fragment can be released upon stimuli, we collected the supernatant from hyperoxia

exposed fibroblasts to treated MLE12 cells for another 24h **(Fig 16 a)**. The treatment, however, did not alter transcription in any of the following genes: *Nrg1*, *Erbb3*, *Aqp5*, *Gata6*, *Hopx*, *Abca3*, *Col1a1*, *Pdgfa*, and *Vegfa* **(Fig 16 b-j)**.

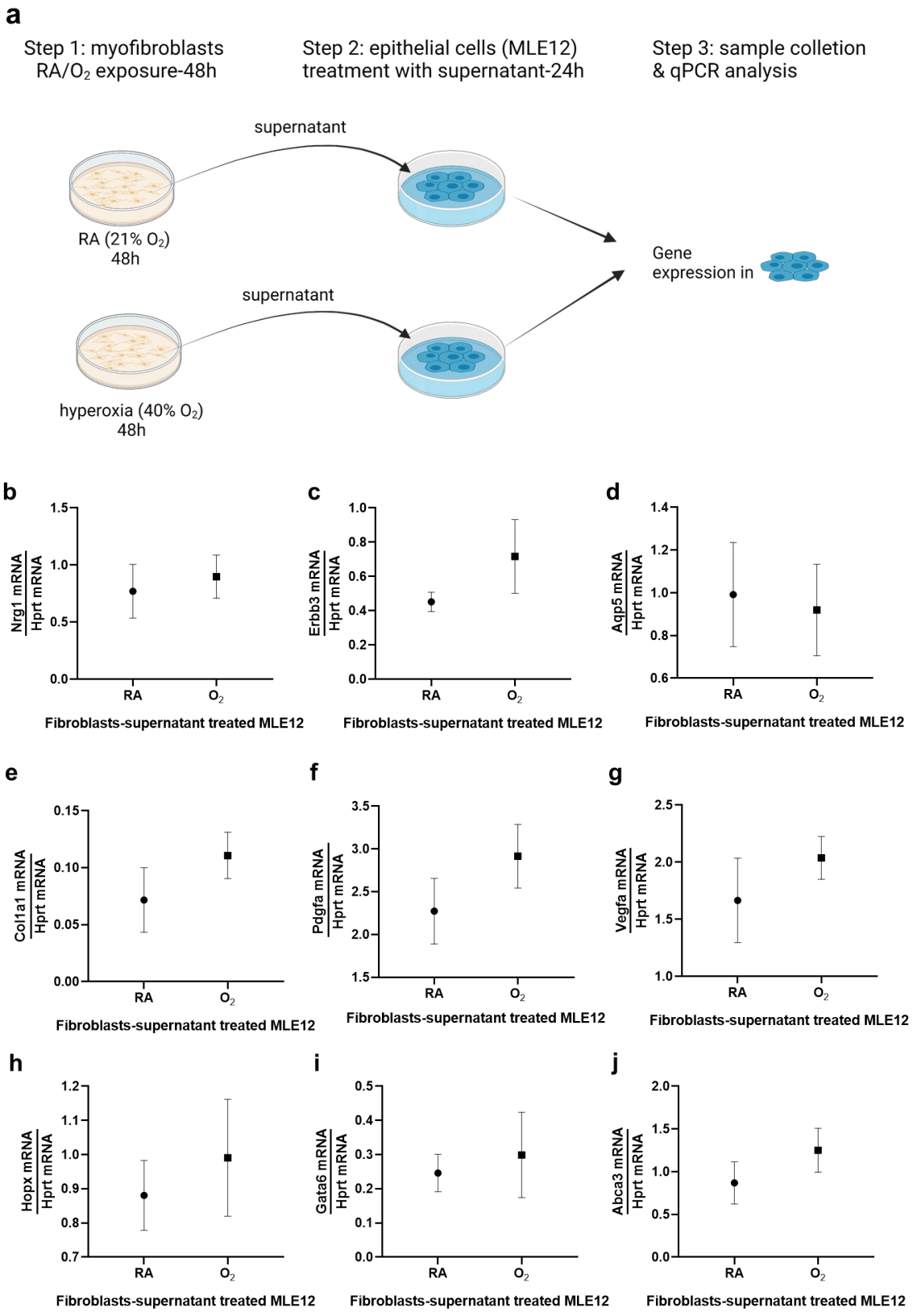

Fig 16 a) Schematic of *in vitro* supernatant treatment mode, Fibroblasts were exposed to 21% or 40% O_2 for 48h, and supernatant were collected from the culture at the end of the exposure and transferred to MLE12 cell cultures. The MLE12 cells were treated for another 24h before sample collection and qPCR analysis; mRNA level in MLE12 cells for **b)** *Nrg1*; **c)** *Erbb3*; **d)** *Aqp5*; **e)** *Col1a1*; **f)** *Pdgfa*; **g)** *Vegfa*; **h)** *Hopx*; **i)** *Gata6*; **j)** *Abca3*, mean ± SD. t-test, *p<0.05, n=3.

4.2.9 Rescue effect of NRG1 treatment on hyperoxia induced inhibition of organoid expansion

Although the transcriptomic changes in monoculture of epithelial cells or fibroblasts in response to hyperoxia exposure were characteristic, it's not possible to speculate how these pathways interact with each other when the two types of cells are in direct or indirect(medium) contact. We then exposed the neonatal organoids (3D co-cultured PMEC and fibroblasts) to hyperoxia in order to assess the dysregulation of ERBB3 pathway and its impact on the hyperoxia induced repression of epithelial cell proliferation. In organoids derived from neonatal PMECs and Mlg cells, 7 days of hyperoxia exposure significantly reduced the organoid size (**Fig 17 a**). Supplementary NRG1 treatment partially counterbalanced the repression effect under hyperoxia **(Fig 17 b)**.

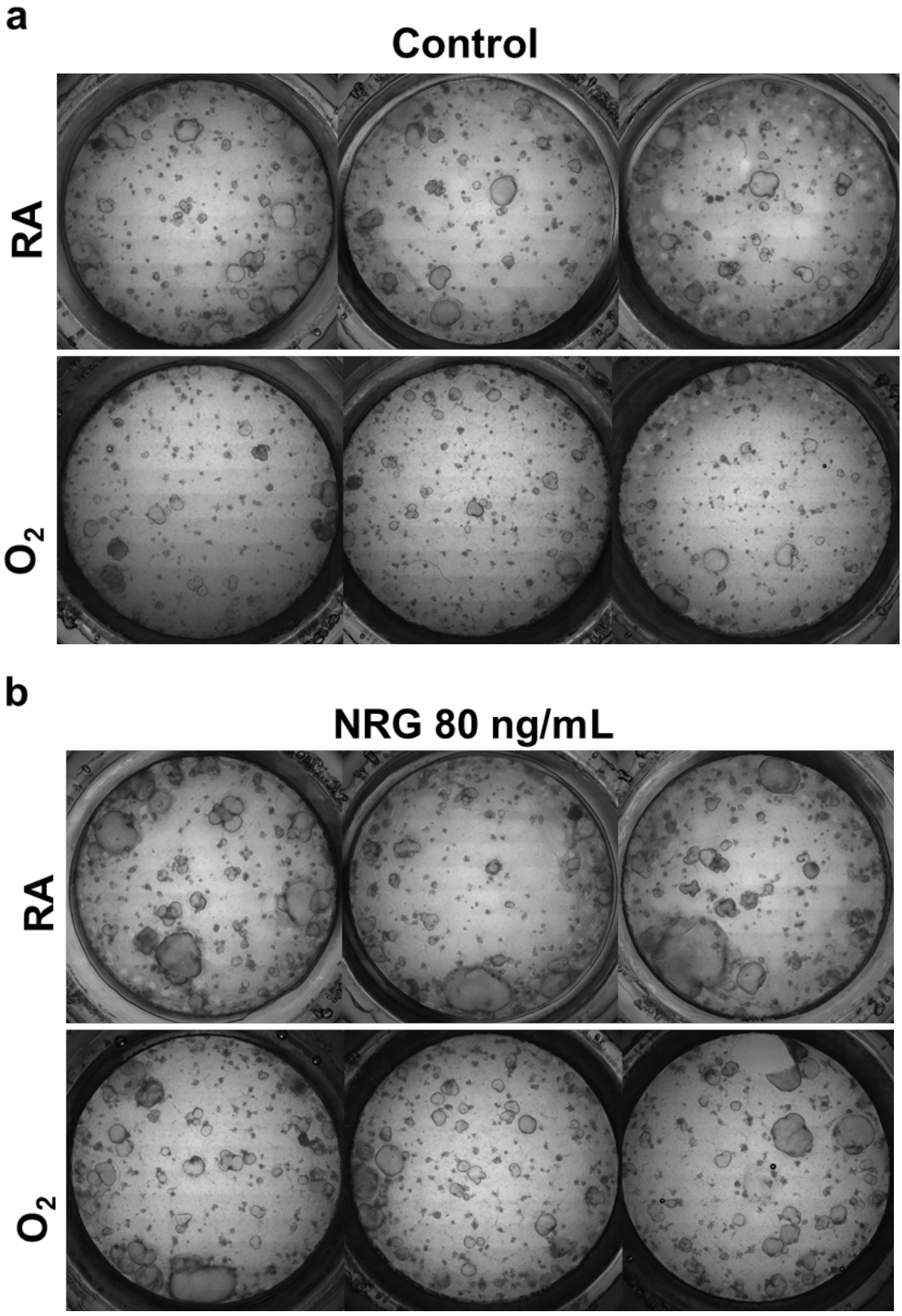

Fig 17. Phase contrast images of neonatal mouse lung organoids after 7-day culture+ 7-day treatment, **a)** medium control, upper panel: RA, lower panel: O_2; **b)** NRG1 80 ng/mL upper panel: RA, lower panel: O_2, 100X, BF.

5. Discussion

5.1 ERBB3 signaling in developing lung

5.1.1 ERBB3 effect on proliferation/differentiation

Our study suggests that ERBB3 receptor is localized in the AEC1 and AEC2 cells of mouse lung peripheral epithelium, alleviates since PND3, and remained at high expression level until PND14. This finding correlates with the time frame of postnatal alveolarization. Co-localized with other crucial components (elastin and PDGF-Rα positive fibroblasts) involved in the secondary septation, phosphorylated ERBB3 is accumulated at the septal tips of postnatal developing lung. We assume the ERBB3 signaling is playing a crucial role in the alveolar epithelium elongation and differentiation.

We tested the ERBB3 phosphorylation at Y1222 residue of intracellular domain. This phosphorylation residue serves as a docking site for p85, a regulatory subunit of Phosphatidylinositol 3-kinase (PI3K) and activates the PI3K/AKT pathway that is closely related to proliferation and cell cycle(Britsch et al. 1998; Roskoski 2014; Wilson et al. 2009). Activation of the ERBB3 in fetal lung explant by NRG1 treatment leads to increased epithelial cell proliferation and volume density, and reduced differentiation (in surfactant production)(Patel et al. 2000). Co-immunoprecipitation of pERBB3 with p85 was detected in proliferating cells. Ligand activation of ERBB increased the pERBB3/p85 complex, and stimulated phosphorylation of Akt and GSK3b, increase in cyclin D1 and cell cycle progression(Sithanandam et al. 2003; Sheng et al. 2010). In our *ex vivo* models, NRG1 treatment also resulted in lung organoid expansion, but not in the colony number.

Therefore, we conclude that ERBB3 activation induced proliferation of alveolar epithelium during secondary septation.

In the *ex vivo* lung organoid model, we isolated the primary epithelial cells with a double negative selection ($CD45^-$/ $CD31^-$). The selected cells were comprised primarily of AEC2, relatively less amount of AEC1 and terminal airway epithelial cells, and a very small cluster of airway and alveolar epithelial progenitors. After 14-days of culture, the organoids could be assigned to two major categories, airway originated (minor) and alveolar originated (major). When treated with NRG1, the organoids revealed a significant increase in AEC1 cell number ($HOPX^+$), also suggesting that ERBB3 activation provoked AEC1 proliferation. Other growth factors such as FGF10 are also reported in negative correlation with AEC1 population size. Knockout of the Fgfr2b, the receptor for FGF10, led to an increase in AEC1 cell numbers and loss of AEC2 cells(Dorry et al. 2020; Liao and Li 2020; Jones et al. 2022; Liberti et al. 2021). Another study reported that postnatal activation of YAP resulted in increased AEC1 numbers(Gokey et al. 2021).

5.1.2 Crosstalk of ERBB3 with PDGF/TGF

The lung mesenchyme comprises several different subtypes of cells, among which myofibroblasts, matrix fibroblasts, lipofibroblasts are the three major populations that are extensively studied in lung development. Other subtypes include smooth muscle cells, mesenchymal stem cells, pericytes, and alveolar niche cells. All three major fibroblast subtypes are PDGF-Rα positive. Lipofibroblasts are marked with THY1, FGF10, TCF21, PDGF-Rα, and FGF18. Lipofibroblasts reside at the base of secondary septae aside to AEC2 and provide triglycerides to AEC2 cells for surfactant synthesis. Another functional feature of lipofibroblasts is FGF10 expression. The FGF10 has been extensively studied in maintaining

the progenitor cells during embryonic branching. Matrix fibroblasts that are marked by DECORIN and COL1A1, on the other hand, contributes predominantly in the ECM production (Riccetti et al. 2020). This fibroblast subtype expresses COL III, COL V, FIBULIN1, FIBULIN2, FIBRILIN2, matrix metalloproteinase (MMP) 3, 17 and 23, and also Lysyl oxidase-like (LOXL) 2 and 4, which crosslink elastin and collagen fibers. The third group, myofibroblasts, marked with TBX4, GLI1, PDGF-Rα, and FGF18, are characterized by α-SMA production, as well as Collagen XIII, XVII, XVIII, and XXIII, integrin, and vinculin (Green et al. 2016). Transdifferentiation of myofibroblast from fibroblast is meditated by the PDGF-Rα. Knockout of the PDGF-Rα resulted in decreased myofibroblast number and alpha-SMA production, leading to abruption of secondary septation(Kimani et al. 2009), while TGFβ counteract against the effects of PDGF-A/PDGF-Rα signaling, enhancing αSMA-abundance(Gouveia, Betsholtz, and Andrae 2018; Horowitz and Thannickal 2006).

In our *ex vivo* organoids, primary epithelial cells from both neonatal and adult mice were co-cultured with the same fibroblast cell line (Mlg). After 14 days of culture, the fibroblasts in neonatal organoids revealed higher expression of PDGF-Rα when compared to the adult, induced by the higher expression of PDGF-A ligand in the neonatal PMEC. The extracellular domain of PDGF-A is shedded by a tumor necrosis factor-alpha converting enzyme (TACE) expressed predominantly by AEC2 and bind the receptor on fibroblasts via paracrine. TACE shedding via zinc-dependent metalloprotease is also reported in the shedding of NRG1, EGF, and TGF-β, which leads to the activation of EGFR/ERBB path-ways(Borrell-Pagès et al. 2003a; Fabregat and Caballero-Díaz 2018; Sunnarborg et al. 2002; Xu et al. 2013; Borrell-Pagès et al. 2003b). It is reported that TACE

is regulated by the ERK (extracellular signal–regulated kinase) or p38 MAPK (mitogen-activated protein kinase) pathway activated by stress (hyperoxia), inflammation, and growth factor(Murphy 2008; Huovila et al. 2005; Lorenzen et al. 2016). Another study indicated that G-protein-coupled receptors (GPCR) activation also leads to the TACE upregulation(George, Hannan, and Thomas 2013).

5.1.3 Impact of the crosstalk on epithelial-mesenchymal cell interaction

Increase in the fibroblast number has resulted in higher organoid forming efficiency in the adult co-culture, but not in the neonate, as we speculate that the fibroblasts initiate the organoid growth. Meanwhile in the neonates, PDGF-A activated the PDGF pathway and induced the differentiation of Mlg cells into myofibroblasts. This increase led to a more predominant role of the fibroblasts in segmenting the organoids, mirroring the septation *in vivo*.

In a gene targeted heterozygous mouse line, attenuated PDGF-Rα expression did not result in direct change of alveolar size or number, but reduced the susceptibility of these mice to hyperoxia and/or mechanical ventilation injury (Oak et al. 2017). Similarly in our *ex vivo* model, the isolated primary fibroblasts from these mice were co-cultured with neonatal PMEC in the *ex vivo* model. The decrease in PDGF-Rα expression did not result in organoid numbers after 14 days of culture. However, when we treated the organoid culture with ERBB3 ligand, the PDGF-Rα$^{+/-}$ group revealed an amplified effect of ERBB3 activation in AEC1 proliferation, as indicated by HOPX positive cell number. Possibly because the reduced PDGF-Rα production repressed the NRG1 shedding and therefore kept ERBB3 signaling at a low level. ERBB3 receptor was upregulated via compensatory negative feedback loop. This finding is also validated *in vivo* that ERBB3

receptor was significantly upregulated in these PDGF-Rα$^{+/-}$ het mouse lungs(Avraham and Yarden 2011).

5.2 ERBB3 regulation under hyperoxia

Hyperoxia is a known pathological factor that contributes to the impaired alveolarization in preterm babies. The oxygen injury disrupts the alveolar epithelium and basement membrane and provoke inflammatory factor release and recruitment of monocyte to the developing lung, and also induce alveolar epithelial-to-mesenchymal cell transition (EMT) via TGF-1β activation(Sunnarborg et al. 2002; Oarhe et al. 2015; Riccetti et al. 2022).

We revealed decreased activation of ERBB3 both *in vivo* and *in vitro* after hyperoxia exposure, and the decrease correlated with reduced proliferation in epithelial cells. Opposite to the receptor downregulation, the ligand (NRG1) was significantly upregulated in monoculture of fibroblasts together with PDGF-Rα and COLLAGEN1, whereas ACTA2, a matrix fibroblast marker was downregulated after hyperoxia exposure. All these changes are less prominent in PDGF-Rα$^{+/-}$ fibroblasts. Both epithelial cells and fibroblasts responded to hyperoxia exposure in ERBB and PDGF signaling. However, the supernatant collected from hyperoxia exposure did not alter ERBB3 signaling in epithelial cell under normoxia, indicating that a dynamic interaction between the two cell types is needed for the NRG1 shedding and ERBB3 activation.

In co-cultured *ex vivo* model, hyperoxia also reduced the epithelial cell proliferation and organoid size, possibly through repressed ERBB3 signaling. NRG1 treatment partially counterbalanced the repression effect under hyperoxia. It is reported that hyperoxia reduces ADAM17/TACE level in epithelial cells (Oarhe et

al. 2015). Our assumption is that hyperoxia reduced the endogenous NRG1 supply by repressing the sheddase activity in TACE, and exogenous treatment of NRG1 was able to compensate the repression.

6. Conclusion and Outlook

This thesis work uncovers new roles of the ErbB3 receptor tyrosine kinase in the alveolarization stage of lung development and disease. In summary, temporal ERBB3 receptors expression in neonatal mouse lung was most prominent during the postnatal alveolarization period (PND3-14) and localized at the septal tip in alveolar epithelial cells. Activation of ERBB3 signaling led to epithelial cell proliferation, indicating a crucial role of ERBB signaling in alveolar epithelium elongation during secondary septation. Epithelial cell-fibroblast interaction was essential in activating ERBB3 signaling. Hyperoxia exposure downregulated ERBB3 signaling in epithelial cells and repressed epithelial cell proliferation, and exogenous NRG1 treatment partially counterbalanced the repression.

Parenchymal and mesenchymal cells at developmental age display distinct physiological and transcriptomic signatures compared to adults. Our *in vivo* and *in vitro* models provided us insights about the ERBB3 pathway signaling in monocultured epithelial cell line as well as in co-culture with fibroblasts. Built on the current understandings, we need to proceed with our research with more components (endothelial cell, immunocyte) for the septation involved in the pathway network, and validate the findings in gene targeted ERBB3$^{+/-}$ transgenic mice.

.

References

Amy, R. W., D. Bowes, P. H. Burri, J. Haines, and W. M. Thurlbeck. 1977. 'Postnatal growth of the mouse lung', *Journal of anatomy*, 124: 131-51.

Andrae, Johanna, Radiosa Gallini, and Christer Betsholtz. 2008. 'Role of platelet-derived growth factors in physiology and medicine', *Genes & Development*, 22: 1276-312.

Appert-Collin, Aline, Pierre Hubert, Gérard Crémel, and Amar Bennasroune. 2015. 'Role of ErbB Receptors in Cancer Cell Migration and Invasion', *Frontiers in Pharmacology*, 6.

Avraham, Roi, and Yosef Yarden. 2011. 'Feedback regulation of EGFR signalling: decision making by early and delayed loops', *Nature Reviews Molecular Cell Biology*, 12: 104-17.

Bellusci, S., R. Henderson, G. Winnier, T. Oikawa, and B. L. Hogan. 1996. 'Evidence from normal expression and targeted misexpression that bone morphogenetic protein (Bmp-4) plays a role in mouse embryonic lung morphogenesis', *Development*, 122: 1693-702.

Betsholtz, C. 1995. 'Role of platelet-derived growth factors in mouse development', *Int J Dev Biol*, 39: 817-25.

Black, Laurel E., Jody F. Longo, and Steven L. Carroll. 2019. 'Mechanisms of Receptor Tyrosine-Protein Kinase ErbB-3 (ERBB3) Action in Human Neoplasia', *The American Journal of Pathology*, 189: 1898-912.

Bland, Richard D., Robert Ertsey, Lucia M. Mokres, Liwen Xu, Berit E. Jacobson, Shu Jiang, Cristina M. Alvira, Marlene Rabinovitch, Eric S. Shinwell, and Anjali Dixit. 2008. 'Mechanical ventilation uncouples synthesis and assembly of elastin and increases apoptosis in lungs of newborn mice', *American Journal of Physiology-Lung Cellular and Molecular Physiology*, 294: L3-L14.

Bonnans, Caroline, Jonathan Chou, and Zena Werb. 2014. 'Remodelling the extracellular matrix in development and disease', *Nature reviews. Molecular cell biology*, 15: 786-801.

Borrell-Pagès, M., F. Rojo, J. Albanell, J. Baselga, and J. Arribas. 2003a. 'TACE is required for the activation of the EGFR by TGF-alpha in tumors', *Embo j*, 22: 1114-24.

Borrell-Pagès, Maria, Federico Rojo, Joan Albanell, Josep Baselga, and Joaquín Arribas. 2003b. 'TACE is required for the activation of the EGFR by TGF-alpha in tumors', *The EMBO Journal*, 22: 1114-24.

Boström, Hans, Karen Willetts, Milos Pekny, Per Levéen, Per Lindahl, Håkan Hedstrand, Marcela Pekna, Mats Hellström, Samuel Gebre-Medhin, Martin Schalling, Mia Nilsson, Siri Kurland, Jan Törnell, John K Heath, and Christer Betsholtz. 1996. 'PDGF-A Signaling Is a Critical Event in Lung Alveolar Myofibroblast Development and Alveogenesis', *Cell*, 85: 863-73.

Britsch, S., L. Li, S. Kirchhoff, F. Theuring, V. Brinkmann, C. Birchmeier, and D. Riethmacher. 1998. 'The ErbB2 and ErbB3 receptors and their ligand, neuregulin-1, are essential for development of the sympathetic nervous system', *Genes & Development*, 12: 1825-36.

Chao, Cho-Ming, Elie El Agha, Caterina Tiozzo, Parviz Minoo, and Saverio Bellusci. 2015. 'A Breath of Fresh Air on the Mesenchyme: Impact of Impaired Mesenchymal Development on the Pathogenesis of Bronchopulmonary Dysplasia', *Frontiers in Medicine*, 2.

Citri, A., K. B. Skaria, and Y. Yarden. 2003. 'The deaf and the dumb: the biology of ErbB-2 and ErbB-3', *Exp Cell Res*, 284: 54-65.

Cybulsky, A. V., A. J. McTavish, J. Papillon, and T. Takano. 1999. 'Role of extracellular matrix and Ras in regulation of glomerular epithelial cell proliferation', *Am J Pathol*, 154: 899-908.

Daley, William P., and Kenneth M. Yamada. 2013. 'ECM-modulated cellular dynamics as a driving force for tissue morphogenesis', *Current opinion in genetics & development*, 23: 408-14.

Desai, Tushar J., Douglas G. Brownfield, and Mark A. Krasnow. 2014. 'Alveolar progenitor and stem cells in lung development, renewal and cancer', *Nature*, 507: 190-94.

Dorry, S. J., B. O. Ansbro, D. M. Ornitz, G. M. Mutlu, and R. D. Guzy. 2020. 'FGFR2 Is Required for AEC2 Homeostasis and Survival after Bleomycin-induced Lung Injury', *Am J Respir Cell Mol Biol*, 62: 608-21.

Fabregat, Isabel, and Daniel Caballero-Díaz. 2018. 'Transforming Growth Factor-β-Induced Cell Plasticity in Liver Fibrosis and Hepatocarcinogenesis', *Frontiers in Oncology*, 8.

Fiaturi, Najla, John J. Castellot, Jr., and Heber C. Nielsen. 2014. 'Neuregulin-ErbB4 signaling in the developing lung alveolus: a brief review', *Journal of cell communication and signaling*, 8: 105-11.

Finigan, James H., Rangnath Mishra, Vihas T. Vasu, Lori J. Silveira, David E. Nethery, Theodore J. Standiford, Ellen L. Burnham, Marc Moss, and Jeffrey A. Kern. 2013. 'Bronchoalveolar lavage neuregulin-1 is elevated in acute lung injury and correlates with inflammation', *European Respiratory Journal*, 41: 396.

George, Amee J., Ross D. Hannan, and Walter G. Thomas. 2013. 'Unravelling the molecular complexity of GPCR-mediated EGFR transactivation using functional genomics approaches', *The FEBS Journal*, 280: 5258-68.

Gokey, Jason J., John Snowball, Anusha Sridharan, Parvathi Sudha, Joseph A. Kitzmiller, Yan Xu, and Jeffrey A. Whitsett. 2021. 'YAP regulates alveolar epithelial cell differentiation and AGER via NFIB/KLF5/NKX2-1', *iScience*, 24: 102967.

Gouveia, Leonor, Christer Betsholtz, and Johanna Andrae. 2018. 'PDGF-A signaling is required for secondary alveolar septation and controls epithelial proliferation in the developing lung', *Development*, 145: dev161976.

Green, Jenna, Mehari Endale, Herbert Auer, and Anne-Karina T. Perl. 2016. 'Diversity of Interstitial Lung Fibroblasts Is Regulated by Platelet-Derived Growth Factor Receptor α Kinase Activity', *American journal of respiratory cell and molecular biology*, 54: 532-45.

Greer, Rachel M., J. Davin Miller, Victor O. Okoh, Brian A. Halloran, and Lawrence S. Prince. 2014. 'Epithelial-mesenchymal co-culture model for studying alveolar morphogenesis', *Organogenesis*, 10: 340-49.

Gumà, Anna, Vicente Martínez-Redondo, Iliana López-Soldado, Carles Cantó, and Antonio Zorzano. 2010. 'Emerging role of neuregulin as a modulator of muscle metabolism', *American Journal of Physiology-Endocrinology and Metabolism*, 298: E742-E50.

Hamilton, T. G., R. A. Klinghoffer, P. D. Corrin, and P. Soriano. 2003. 'Evolutionary divergence of platelet-derived growth factor alpha receptor signaling mechanisms', *Mol Cell Biol*, 23: 4013-25.

Herrlich, Andreas, Eva Klinman, Jonathan Fu, Cameron Sadegh, and Harvey Lodish. 2008. 'Ectodomain cleavage of the EGF ligands HB-EGF, neuregulin1-β, and TGF-α is specifically triggered by different stimuli and involves different PKC isoenzymes', *The FASEB Journal*, 22: 4281-95.

Higashiyama, Shigeki, Daisuke Nanba, Hironao Nakayama, Hirofumi Inoue, and Shinji Fukuda. 2011. 'Ectodomain shedding and remnant peptide signalling of EGFRs and their ligands', *The Journal of Biochemistry*, 150: 15-22.

Horowitz, Jeffrey C., and Victor J. Thannickal. 2006. 'Epithelial-mesenchymal interactions in pulmonary fibrosis', *Seminars in respiratory and critical care medicine*, 27: 600-12.

Huang, Zheping, Yulian Wang, Pritha S. Nayak, Christiane E. Dammann, and Juan Sanchez-Esteban. 2012. 'Stretch-induced Fetal Type II Cell Differentiation Is Mediated via ErbB1-ErbB4 Interactions *', *Journal of Biological Chemistry*, 287: 18091-102.

Huovila, Ari-Pekka J., Anthony J. Turner, Markku Pelto-Huikko, Iivari Kärkkäinen, and Rebekka M. Ortiz. 2005. 'Shedding light on ADAM metalloproteinases', *Trends in Biochemical Sciences*, 30: 413-22.

Hussain, Musaddique, Chengyun Xu, Mashaal Ahmad, Youping Yang, Meiping Lu, Xiling Wu, Lanfang Tang, and Ximei Wu. 2017. 'Notch Signaling: Linking Embryonic Lung Development and Asthmatic Airway Remodeling', *Molecular Pharmacology*, 92: 676-93.

Iwakura, Yuriko, Ran Wang, Naoko Inamura, Kazuaki Araki, Shigeki Higashiyama, Nobuyuki Takei, and Hiroyuki Nawa. 2017. 'Glutamate-dependent ectodomain shedding of neuregulin-1 type II precursors in rat forebrain neurons', *PLOS ONE*, 12: e0174780.

Jones, Matthew R., Lei Chong, Arun Reddy Limgapally, Jochen Wilhem, Meshal Ansari, Herbert B. Schiller, Gianni Carraro, and Saverio Bellusci. 2022. 'Characterization of alveolar epithelial lineage heterogeneity during the late pseudoglandular stage of mouse lung development', *bioRxiv*: 2022.01.05.475053.

Kalikkot Thekkeveedu, Renjithkumar, Milenka Cuevas Guaman, and Binoy Shivanna. 2017. 'Bronchopulmonary dysplasia: A review of pathogenesis and pathophysiology', *Respiratory Medicine*, 132: 170-77.

Kimani, Patricia W., Amey J. Holmes, Ruth E. Grossmann, and Stephen E. McGowan. 2009. 'PDGF-Rα gene expression predicts proliferation, but PDGF-A suppresses transdifferentiation of neonatal mouse lung myofibroblasts', *Respiratory Research*, 10: 119.

Kuang, Ping-Ping, Xiao-Hui Zhang, Celeste B. Rich, Judith A. Foster, Mangalalaxmy Subramanian, and Ronald H. Goldstein. 2007. 'Activation of elastin transcription by transforming growth factor-β in human lung fibroblasts', *American Journal of Physiology-Lung Cellular and Molecular Physiology*, 292: L944-L52.

Lee, K. F., H. Simon, H. Chen, B. Bates, M. C. Hung, and C. Hauser. 1995. 'Requirement for neuregulin receptor erbB2 in neural and cardiac development', *Nature*, 378: 394-8.

Lemmon, Mark A. 2009. 'Ligand-induced ErbB receptor dimerization', *Experimental Cell Research*, 315: 638-48.

Liao, Danying, and Huaibiao Li. 2020. 'Dissecting the Niche for Alveolar Type II Cells With Alveolar Organoids', *Frontiers in Cell and Developmental Biology*, 8.

Liberti, D. C., M. M. Kremp, W. A. Liberti, 3rd, I. J. Penkala, S. Li, S. Zhou, and E. E. Morrisey. 2021. 'Alveolar epithelial cell fate is maintained in a spatially restricted manner to promote lung regeneration after acute injury', *Cell Rep*, 35: 109092.

Lindahl, P., L. Karlsson, M. Hellström, S. Gebre-Medhin, K. Willetts, J. K. Heath, and C. Betsholtz. 1997. 'Alveogenesis failure in PDGF-A-deficient mice is coupled to lack of distal spreading of alveolar smooth muscle cell progenitors during lung development', *Development*, 124: 3943-53.

Lorenzen, Inken, Juliane Lokau, Yvonne Korpys, Mirja Oldefest, Charlotte M. Flynn, Ulrike Künzel, Christoph Garbers, Matthew Freeman, Joachim Grötzinger, and Stefan Düsterhöft. 2016. 'Control of ADAM17 activity by regulation of its cellular localisation', *Scientific Reports*, 6: 35067.

Lu, P., K. Takai, V. M. Weaver, and Z. Werb. 2011. 'Extracellular matrix degradation and remodeling in development and disease', *Cold Spring Harb Perspect Biol*, 3.

Lwebuga-Mukasa, J. S. 1991. 'Matrix-driven pneumocyte differentiation', *Am Rev Respir Dis*, 144: 452-7.

Malleske, Daniel T., Don Hayes, Scott W. Lallier, Cynthia L. Hill, and Susan D. Reynolds. 2018. 'Regulation of Human Airway Epithelial Tissue Stem Cell Differentiation by β-Catenin, P300, and CBP', *Stem Cells*, 36: 1905-16.

Mattfeldt, T., H. J. Möbius, and G. Mall. 1985. 'Orthogonal triplet probes: an efficient method for unbiased estimation of length and surface of objects with unknown orientation in space', *J Microsc*, 139: 279-89.

McGowan, S. E., R. E. Grossmann, P. W. Kimani, and A. J. Holmes. 2008. 'Platelet-derived growth factor receptor-alpha-expressing cells localize to the alveolar entry ring and have characteristics of myofibroblasts during pulmonary alveolar septal formation', *Anat Rec (Hoboken)*, 291: 1649-61.

Metzger, Ross J., Ophir D. Klein, Gail R. Martin, and Mark A. Krasnow. 2008. 'The branching programme of mouse lung development', *Nature*, 453: 745-50.

Mishra, Rangnath, Daniel G. Foster, James H. Finigan, and Jeffrey A. Kern. 2019. 'Interleukin-6 is required for Neuregulin-1 induced HER2 signaling in lung epithelium', *Biochemical and biophysical research communications*, 513: 794-99.

Morrow, Lindsey A., Brandie D. Wagner, David A. Ingram, Brenda B. Poindexter, Kurt Schibler, C. Michael Cotten, John Dagle, Marci K. Sontag, Peter M. Mourani, and Steven H. Abman. 2017. 'Antenatal Determinants of Bronchopulmonary Dysplasia and Late Respiratory Disease in Preterm Infants', *American Journal of Respiratory and Critical Care Medicine*, 196: 364-74.

Mund, Sonja I., Marco Stampanoni, and Johannes C. Schittny. 2008. 'Developmental alveolarization of the mouse lung', *Developmental Dynamics*, 237: 2108-16.

Murphy, G. 2008. 'The ADAMs: signalling scissors in the tumour microenvironment', *Nat Rev Cancer*, 8: 929-41.

Nagasaka, Misako, and Sai-Hong Ignatius Ou. 2022. 'NRG1 and NRG2 fusion positive solid tumor malignancies: a paradigm of ligand-fusion oncogenesis', *Trends in Cancer*, 8: 242-58.

Nasri, Amel, Florent Foisset, Engi Ahmed, Zakaria Lahmar, Isabelle Vachier, Christian Jorgensen, Said Assou, Arnaud Bourdin, and John De Vos. 2021. 'Roles of Mesenchymal Cells in the Lung: From Lung Development to Chronic Obstructive Pulmonary Disease', *Cells*, 10: 3467.

Negretti, N. M., E. J. Plosa, J. T. Benjamin, B. A. Schuler, A. C. Habermann, C. S. Jetter, P. Gulleman, C. Bunn, A. N. Hackett, M. Ransom, C. J. Taylor, D. Nichols, B. K. Matlock, S. H. Guttentag, T. S. Blackwell, N. E. Banovich, J. A. Kropski, and J. M. S. Sucre. 2021. 'A single-cell atlas of mouse lung development', *Development*, 148.

Nikolić, Marko Z., Dawei Sun, and Emma L. Rawlins. 2018. 'Human lung development: recent progress and new challenges', *Development*, 145: dev163485.

Oak, P., T. Pritzke, I. Thiel, M. Koschlig, D. S. Mous, A. Windhorst, N. Jain, O. Eickelberg, K. Foerster, A. Schulze, W. Goepel, T. Reicherzer, H. Ehrhardt, R. J. Rottier, P. Ahnert, L. Gortner, T. J. Desai, and A. Hilgendorff. 2017. 'Attenuated PDGF signaling drives alveolar and microvascular defects in neonatal chronic lung disease', *EMBO Mol Med*, 9: 1504-20.

Oarhe, Chinyere I., Vinh Dang, MyTrang Dang, Hang Nguyen, Indiwari Gopallawa, Ira H. Gewolb, and Bruce D. Uhal. 2015. 'Hyperoxia downregulates angiotensin-converting enzyme-2 in human fetal lung fibroblasts', *Pediatric Research*, 77: 656-62.

Olayioye, Monilola A., Richard M. Neve, Heidi A. Lane, and Nancy E. Hynes. 2000. 'The ErbB signaling network: receptor heterodimerization in development and cancer', *The EMBO Journal*, 19: 3159-67.

Olsen, Colin E., Brant E. Isakson, Gregory J. Seedorf, Richard L. Lubman, and Scott Boitano. 2005. 'EXTRACELLULAR MATRIX-DRIVEN ALVEOLAR EPITHELIAL CELL DIFFERENTIATION IN VITRO', *Experimental Lung Research*, 31: 461-82.

Ostrin, E. J., D. R. Little, K. N. Gerner-Mauro, E. A. Sumner, R. Ríos-Corzo, E. Ambrosio, S. E. Holt, N. Forcioli-Conti, H. Akiyama, S. M. Hanash, S. Kimura, S. X. L. Huang, and J. Chen. 2018. 'β-Catenin maintains lung epithelial progenitors after lung specification', *Development*, 145.

Patel, N. V., M. J. Acarregui, J. M. Snyder, J. M. Klein, M. X. Sliwkowski, and J. A. Kern. 2000. 'Neuregulin-1 and human epidermal growth factor receptors 2 and 3 play a role in human lung development in vitro', *Am J Respir Cell Mol Biol*, 22: 432-40.

Perl, Anne-Karina T., and Emily Gale. 2009. 'FGF signaling is required for myofibroblast differentiation during alveolar regeneration', *American Journal of Physiology-Lung Cellular and Molecular Physiology*, 297: L299-L308.

Riccetti, Matthew, Jason J. Gokey, Bruce Aronow, and Anne-Karina T. Perl. 2020. 'The elephant in the lung: Integrating lineage-tracing, molecular markers, and single cell sequencing data to identify distinct fibroblast populations during lung development and regeneration', *Matrix biology : journal of the International Society for Matrix Biology*, 91-92: 51-74.

Riccetti, Matthew R., Mereena George Ushakumary, Marion Waltamath, Jenna Green, John Snowball, Sydney E. Dautel, Mehari Endale, Bonny Lami, Jason Woods, Shawn K. Ahlfeld, and Anne-Karina T. Perl. 2022. 'Maladaptive functional changes in alveolar fibroblasts due to perinatal hyperoxia impair epithelial differentiation', *JCI Insight*, 7.

Riethmacher, D., E. Sonnenberg-Riethmacher, V. Brinkmann, T. Yamaai, G. R. Lewin, and C. Birchmeier. 1997. 'Severe neuropathies in mice with targeted mutations in the ErbB3 receptor', *Nature*, 389: 725-30.

Rodríguez-Castillo, José Alberto, David Bravo Pérez, Aglaia Ntokou, Werner Seeger, Rory E. Morty, and Katrin Ahlbrecht. 2018. 'Understanding alveolarization to induce lung regeneration', *Respiratory Research*, 19: 148.

Roskoski, R., Jr. 2014. 'The ErbB/HER family of protein-tyrosine kinases and cancer', *Pharmacol Res*, 79: 34-74.

Schittny, Johannes C. 2017. 'Development of the lung', *Cell and Tissue Research*, 367: 427-44.

Schmelzer, Eva, Vitale Miceli, Cinzia Maria Chinnici, Alessandro Bertani, and Jörg C. Gerlach. 2020. 'Effects of Mesenchymal Stem Cell Coculture on Human Lung Small Airway Epithelial Cells', *BioMed Research International*, 2020: 9847579.

Schulze, Waltraud X., Lei Deng, and Matthias Mann. 2005. 'Phosphotyrosine interactome of the ErbB-receptor kinase family', *Molecular systems biology*, 1: 2005.0008-2005.0008.

Sheng, Q., X. Liu, E. Fleming, K. Yuan, H. Piao, J. Chen, Z. Moustafa, R. K. Thomas, H. Greulich, A. Schinzel, S. Zaghlul, D. Batt, S. Ettenberg, M. Meyerson, B. Schoeberl, A. L. Kung, W. C. Hahn, R. Drapkin, D. M. Livingston, and J. F. Liu. 2010. 'An activated ErbB3/NRG1 autocrine loop supports in vivo proliferation in ovarian cancer cells', *Cancer Cell*, 17: 298-310.

Sithanandam, G., G. T. Smith, A. Masuda, T. Takahashi, L. M. Anderson, and L. W. Fornwald. 2003. 'Cell cycle activation in lung adenocarcinoma cells by the ErbB3/phosphatidylinositol 3-kinase/Akt pathway', *Carcinogenesis*, 24: 1581-92.

Sivakumar, A., and D. B. Frank. 2019. 'Paradigms that define lung epithelial progenitor cell fate in development and regeneration', *Curr Stem Cell Rep*, 5: 133-44.

Sliwkowski, M. X., G. Schaefer, R. W. Akita, J. A. Lofgren, V. D. Fitzpatrick, A. Nuijens, B. M. Fendly, R. A. Cerione, R. L. Vandlen, and K. L. Carraway, 3rd. 1994. 'Coexpression of erbB2 and erbB3 proteins reconstitutes a high affinity receptor for heregulin', *J Biol Chem*, 269: 14661-5.

Spanò, D. P., and S. D. Scilabra. 2022. 'Tissue Inhibitor of Metalloproteases 3 (TIMP-3): In Vivo Analysis Underpins Its Role as a Master Regulator of Ectodomain Shedding', *Membranes (Basel)*, 12.

Sunnarborg, S. W., C. L. Hinkle, M. Stevenson, W. E. Russell, C. S. Raska, J. J. Peschon, B. J. Castner, M. J. Gerhart, R. J. Paxton, R. A. Black, and D. C. Lee. 2002. 'Tumor necrosis factor-alpha converting enzyme (TACE) regulates epidermal growth factor receptor ligand availability', *J Biol Chem*, 277: 12838-45.

Tao, Rong-Hua, and Ichi N. Maruyama. 2008. 'All EGF(ErbB) receptors have preformed homo- and heterodimeric structures in living cells', *Journal of Cell Science*, 121: 3207-17.

Treutlein, Barbara, Doug G. Brownfield, Angela R. Wu, Norma F. Neff, Gary L. Mantalas, F. Hernan Espinoza, Tushar J. Desai, Mark A. Krasnow, and Stephen R. Quake. 2014. 'Reconstructing lineage hierarchies of the distal lung epithelium using single-cell RNA-seq', *Nature*, 509: 371-75.

Ushakumary, Mereena George, Matthew Riccetti, and Anne-Karina T. Perl. 2021. 'Resident interstitial lung fibroblasts and their role in alveolar stem cell niche development, homeostasis, injury, and regeneration', *Stem cells translational medicine*, 10: 1021-32.

Váradi, Tímea, Magdalena Schneider, Eva Sevcsik, Dominik Kiesenhofer, Florian Baumgart, Gyula Batta, Tamás Kovács, René Platzer, Johannes B. Huppa, János Szöllősi, Gerhard J. Schütz, Mario Brameshuber, and Peter Nagy. 2019. 'Homo- and Heteroassociations Drive Activation of ErbB3', *Biophysical Journal*, 117: 1935-47.

Volckaert, Thomas, and Stijn P. De Langhe. 2015. 'Wnt and FGF mediated epithelial-mesenchymal crosstalk during lung development', *Developmental Dynamics*, 244: 342-66.

Weaver, M., L. Batts, and B. L. Hogan. 2003. 'Tissue interactions pattern the mesenchyme of the embryonic mouse lung', *Dev Biol*, 258: 169-84.

Weaver, M., N. R. Dunn, and B. L. Hogan. 2000. 'Bmp4 and Fgf10 play opposing roles during lung bud morphogenesis', *Development*, 127: 2695-704.

Wilson, Kristy J., Jennifer L. Gilmore, John Foley, Mark A. Lemmon, and David J. Riese. 2009. 'Functional selectivity of EGF family peptide growth factors: Implications for cancer', *Pharmacology & Therapeutics*, 122: 1-8.

Xu, Keli, Erica Nieuwenhuis, Brenda L. Cohen, Wei Wang, Angelo J. Canty, Jayne S. Danska, Leigh Coultas, Janet Rossant, Megan Y. J. Wu, Tino D. Piscione, Andras Nagy, Achim Gossler, Geoff G. Hicks, Chi-Chung Hui, R. Mark Henkelman, Lisa X. Yu, John G. Sled, Thomas Gridley, and Sean E. Egan. 2009. 'Lunatic Fringe-mediated Notch signaling is required for lung alveogenesis', *American Journal of Physiology-Lung Cellular and Molecular Physiology*, 298: L45-L56.

Xu, Wei, Chengyu Liu, Vesa Kaartinen, Hui Chen, Chi-Han Lu, Wenming Zhang, Yongfeng Luo, and Wei Shi. 2013. 'TACE in perinatal mouse lung epithelial cells promotes lung saccular formation', *American Journal of Physiology-Lung Cellular and Molecular Physiology*, 305: L953-L63.

Yamada, Kohta, Takeru Hamashima, Yoko Ishii, Yamamoto, Seiji, Noriko Okuno, Naofumi Yoshida, Moe Yamada, Ting Huang, Ting, Norifumi Shioda, Kei Tomihara, Toshihiko Fujimori, Hisashi Mori, Kohji Fukunaga, Makoto Noguchi, and Masakiyo Sasahara. 2018. 'Different PDGF Receptor Dimers Drive Distinct Migration Modes of the Mouse Skin Fibroblast', *Cellular Physiology and Biochemistry*, 51: 1461-79.

Yin, Z., L. Gonzales, V. Kolla, N. Rath, Y. Zhang, M. M. Lu, S. Kimura, P. L. Ballard, M. F. Beers, J. A. Epstein, and E. E. Morrisey. 2006. 'Hop functions downstream of Nkx2.1 and GATA6 to mediate HDAC-dependent negative regulation of pulmonary gene expression', *Am J Physiol Lung Cell Mol Physiol*, 291: L191-9.

Yuan, Tingting, Thomas Volckaert, Diptiman Chanda, Victor J. Thannickal, and Stijn P. De Langhe. 2018. 'Fgf10 Signaling in Lung Development, Homeostasis, Disease, and Repair After Injury', *Frontiers in genetics*, 9: 418-18.

List of abbreviations

ABCA3	ATP Binding Cassette Subfamily A Member 3
ADAM	a disintegrin and metalloproteinase
AEs	airway epithelial cells
AEC1	alveolar type 1 cells
AEC2	alveolar type 2 cells
AQP5	Aquaporin 5
BMP4	Bone Morphogenic Protein 4
BPD	Bronchopulmonary dysplasia
BW	body weight
CD31	Platelet endothelial cell adhesion molecule (PECAM-1)
CD45	Protein tyrosine phosphatase, receptor type, C
cDNA	complementary deoxyribonucleic acid
CFE	colony forming efficiency
CO_2	carbon dioxide
COL1A1	Collagen Type I Alpha 1 Chain
Ct	cycle threshold
DAB	3,3′-Diaminobenzidine
DAPI	4′,6-diamidino-2-phenylindole
DBE	dibenzyl ether
DMEM	Dulbecco's Modified Eagle's Medium
DMSO	dimethyl sulfoxide
ECM	extracellular matrix
EDTA	Ethylenediaminetetraacetic acid

EGF	epidermal growth factors
EGFR	Epidermal growth factor receptor
EHS	Engelbreth-Holm-Swarm mouse
ERBB2	Receptor tyrosine-protein kinase erbB-2
ERBB3	Receptor tyrosine-protein kinase erbB-3
ERBB4	Receptor tyrosine-protein kinase erbB-4
ERK	extracellular signal-regulated kinases
FBS	Fetal bovine serum
FFPE	formalin fixed paraffin embedded
FGF	Fibroblast growth factors
FiO_2	Fraction of inspired oxygen
GATA6	GATA Binding Protein 6
GPCR	G-protein-coupled receptors
HOPX	homeodomain-only protein
HPF	high-power field
Hprt	hypoxanthine-guanine phosphoribosyl transferase
HRG	Heregulin
ICAM1	intercellular adhesion molecule 1
IF	immunofluorescence
IHC	immunohistochemistry
Ln5	laminin-5
LSFM	light sheet fluorescent microscopy
Lox	Lysyl oxidase-like

MAPK	mitogen-activated protein kinase
MFB	myofibroblasts
MLE12	Murine lung epithelial cell line
Mlg	murine lung fibroblasts cell line
MMP	metaloproteinase
mRNA	messenger ribonucleic acid
MSCs	mesenchymal stem cells
MUC1	mucin
NA	numerical aperture
NRG	neuregulins
PBS	Phosphate-buffered saline
PBSG-T	PBS-Gelatin-Triton X-100 buffer
PBST	phosphate-buffered saline solution with a low-concentration detergent solution
PCR	polymerase chain reaction
PDGF-A	platelet-derived growth factor A
PDGF-Rα	platelet-derived growth factor receptor alpha
PDPN	Podoplanin
PET	polyester
PFA	paraformaldehyde
PI3K	Phosphatidylinositol 3-kinase
PMECs	Primary mouse epithelial cells
PND	Postnatal days
qPCR	quantitative real-time polymerase chain reaction
RA	room air (21% O_2)
RIPA	Radioimmunoprecipitation assay buffer

RNA	ribonucleic acid
rpm	revolutions per minute
RT	room temperature
RTK	receptor tyrosine kinases
SD	standard deviation
shh	sonic hedgehog
SP-C	surfactant protein C
TACE	tumor necrosis factor-alpha converting enzyme
TBS-T	tris-buffered saline with a low-concentration detergent solution
TGF-β	Transforming growth factor-β
THF	tetrahydrofuran
VEGF-A	Vascular Endothelial Growth Factor A
WB	western blot
WT	wildtype
α-SMA	α-smooth muscle actin

Acknowledgements

I would like to express my deepest appreciation to Dr. Anne Hilgendorff, for providing me with this opportunity to complete my study in her lab, and for encouraging and guiding me through all the confusion and challenges. Her expertise and dedication to pediatric science gave me great inspiration towards my project and future career.

I would also like to express my sincere gratitude to my thesis committee members, Prof. Dr. Michael O'Reilly, Dr. Tobias Stöger, and Prof. Dr. Thomas Gudermann, for their insightful comments and suggestions at every stage of the research project.

I am also very grateful to the graduate program “GRK 2338” and the CPC research school for their training and support of my study in the Comprehensive Pneumology Center. Special thanks to Dr. Claudia Staab-Weijnitz, Dr. Julia Brandt, and Stefanie Resenberger, for their great effort in assisting every PhD student throughout the process.

I am grateful to all the previous and current members of the AH group: Erika Gonzalez Rodriguez, Anna Dmitrieva, Motaharehsadat Heydarian, Prajakta Oak, Carola Voss, Julia Waiden, Juliane Schneider, Mircea-Gabriel Stoleriu, Susanne Mehring, Elisabeth Schindler, Aakruti Nayak, Lena Haist, Friederike Haefner, and Inga Meincke, for their scientific input, technical support, and also friendship and good times.

My special thanks to my fellow PhD students, in particular Qianjiang Hu, for their selfless sharing of knowledge, experiences, and advice on the daily lab work.

Furthermore, I am very thankful for all the support that I received from my collaboration partners, Prof. Jennifer Sucre, Dr Carola Voss, Dr. Otmar Schmid, Dr. Lin Yang, Dr. Qiongliang Liu,

Finally, to my dearest parents and friends for their unconditional love and understanding.

Affidavit

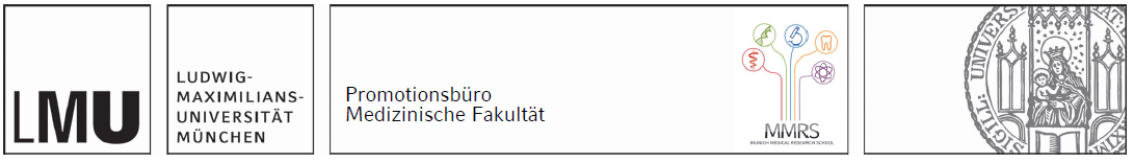

Affidavit

Role of ERBB3 in the interplay between epithelial cells and fibroblasts during late-stage lung development and disease

Zhang Xin

Surname, first name

Street

Zip code, town, country

I hereby declare, that the submitted thesis entitled:

……

is my own work. I have only used the sources indicated and have not made unauthorized use of services of a third party. Where the work of others has been quoted or reproduced, the source is always given.

I further declare that the submitted thesis or parts thereof have not been presented as part of an examination degree to any other university.

Shanghai, Dec 20th, 2022

place, date

Xin Zhang

Signature doctoral candidate

Confirmation of congruency

LMU LUDWIG-MAXIMILIANS-UNIVERSITÄT MÜNCHEN

Promotionsbüro Medizinische Fakultät

MMRS

Confirmation of congruency between printed and electronic version of the doctoral thesis

Role of ERBB3 in the interplay between epithelial cells and fibroblasts during late-stage lung development and disease

Zhang Xin

Surname, first name

Street

Zip code, town, country

I hereby declare, that the submitted thesis entitled:

……

is congruent with the printed version both in content and format.

Shanghai, Dec 20th, 2022

place, date

Xin Zhang

Signature doctoral candidate